공학석사학위논문

수소전기버스 연료전지 시스템 모델링

Modeling of PEM fuel cell system of a fuel cell electric bus

2023 년 8 월

서울대학교 대학원
기계공학부
김 영 섭

수소전기버스 연료전지 시스템 모델링

Modeling of PEM fuel cell system of a fuel cell electric bus

지도교수 민 경 덕

이 논문을 공학석사 학위논문으로 제출함

2023 년 4 월

서울대학교 대학원
기계공학부
김 영 섭

김 영 섭의 공학석사 학위논문을 인준함

2023 년 6 월

위 원 장 : 김 찬 중 (인)

부위원장 : 민경덕 (인)

위 원 : 송한호 (인)

Abstract

Modeling of PEM fuel cell system

of a fuel cell electric bus

Youngseob Kim

Department of Mechanical Engineering

The Graduate School

Seoul National University

The fuel cell electric bus (FCEB) is a hybrid vehicle equipped with both a fuel cell and a battery, showcasing eco-friendliness and low noise characteristics. Recently, it has gained attention for its ability to simplify hydrogen charging and maintenance infrastructure. Additionally, the high energy density of hydrogen enhances the vehicle's energy storage capacity and mileage, making it suitable for various transportation modes, including trucks and buses.

The polymer electrolyte membrane (PEM) fuel cell in the fuel cell electric bus (FCEB) serves as an energy conversion device, transforming the chemical energy of hydrogen into electrical energy, with water and heat produced as by-products through electrochemical reactions. The PEM fuel cell system comprises the PEM fuel cell stack and the balance of plant (BOP) system. The BOP system includes components

like an air supply system for oxygen and hydrogen, a reactor, a hydrogen supply system, and a thermal management system (TMS) to regulate the fuel cell's operating temperature between 60℃ to 80℃.

For this study, the FCEB PEM fuel cell system was modeled using AMESIM®, and the simulation model was validated with FCEB vehicle test data. The PEM fuel cell system, which encompasses the PEM fuel cell stack, air compressor, and membrane humidifier, was accurately modeled. The PEM fuel cell single cell and stack simulation model exhibited errors within 1% and 2%, respectively, when compared to the polarization curve. The simulation model of the air compressor closely matched the test values with an error within 2%, considering temperature and pressure results. Furthermore, the TMS simulation model showed good agreement with errors within 3.4% when compared to the test values, particularly concerning coolant mass flow rate and temperature results. The overall fuel cell system was verified by calculating the power and power consumption of each component, and the energy flow simulation results closely resembled the dynamometer vehicle test data.

Keyword: Fuel cell electric bus, PEM fuel cell, BOP system, Simulation

Student Number: 2021-24465

Table of Contents

List of Figures

List of Tables

Nomenclature

PEMFC	*Polymer electrolyte membrane fuel cell*
FCEB	*Fuel cell electric bus*
MEA	*Membrane electrode assembly*
GDL	*Gas diffusion layer*
BOP	*Balance of plant*
TMS	*Thermal management system*
RH	*Relative humidity, %*

Chapter 1. Introduction

1.1. Background

The polymer electrolyte membrane (PEM) fuel cells have found extensive applications in various modes of transportation, including vehicles, ships, and airplanes. The high energy density of hydrogen significantly enhances the energy storage capacity and vehicle mileage, making it particularly valuable for trucks, buses, and other means of transportation [1].

The PEM fuel cell system mainly consists of two major components: the PEM fuel cell stack and the balance of plant (BOP) system. The PEM fuel cell serves as an energy conversion device that transforms the chemical energy of hydrogen into electrical energy, generating water and heat as by-products through electrochemical reactions. Consequently, the BOP system includes an air supply system for delivering oxygen and a hydrogen supply system, along with a thermal management system (TMS) to maintain the fuel cell's operating temperature at an appropriate level [2,3]. The BOP system configuration is presented in Fig. 1.1.

The PEM fuel cell system consists of the following components:

1. Fuel Cell Stack: The heart of the system, containing multiple individual PEM fuel cells stacked together. Each fuel cell consists of an anode, a cathode, and a proton exchange membrane that facilitates the electrochemical reaction.

2. Fuel Supply: Provides a continuous flow of hydrogen gas to the anode side of the fuel cell stack.

3. Air Supply: Supplies oxygen or air to the cathode side of the fuel cell stack.

4. Reactant Humidification: Ensures the reactant gases are properly humidified to improve the efficiency of the electrochemical reaction.

5. TMS: Manages the heat generated during the electrochemical process to maintain the optimal operating temperature of the fuel cell.

6. Power Conditioning Unit: Converts the direct current (DC) output from the fuel cell stack into alternating current (AC) suitable for powering various electrical devices.

The PEM fuel cell system efficiently converts the chemical energy of hydrogen into electrical energy, generating water and heat as byproducts, thus establishing itself as a clean and environmentally friendly power generation technology.

The hydrogen supply system incorporates an on/off valve responsible for supplying or shutting off hydrogen from the hydrogen tank through the hydrogen shut-off valve. This valve opens upon starting and closes when the system is turned off. The amount of hydrogen delivered to the stack is controlled by regulating the current through the hydrogen supply valve. Additionally, the ejector recirculates unreacted hydrogen by drawing a mixture of gas from the stack outlet. Managing the hydrogen concentration within the stack is achieved through the use of a purge valve, which enables water generated by the fuel cell reaction to pass through the membrane due to concentration differences. The water then turns into liquid in the anode, flowing down to the water trap through gravity, and discharging to the outside through the drain valve when a certain water level is reached. The residual air and moisture from the cathode outlet are utilized to humidify the dry air passing through the humidifier and entering the cathode inlet [2,3].

The air supply system effectively eliminates impurities via an air cleaner, providing the required air for the fuel cell stack reaction at an appropriate flow rate and pressure using an air compressor. To ensure optimal performance and durability of the fuel cell, the humidifier maintains the suitable humidity level within the fuel cell. Additionally, the opening of the valve is adjusted based on external air conditions using the operating pressure control device to pressurize the PEM fuel cell stack [3].

The cathode oxygen depletion (COD) heater in the heat management system preheats the coolant during cold starts and removes any remaining oxygen and hydrogen from the stack. The coolant flows through the coolant pump, and as the stack operates, the coolant is cooled through the radiator when its temperature rises. Furthermore, the ion filter is responsible for filtering the coolant ions, ensuring the vehicle's electrical conductivity and overall electrical stability [4]. The TMS system is depicted in Fig. 1.2.

Fig. 1.1 Schematic diagram of PEM fuel cell stack and BOP system

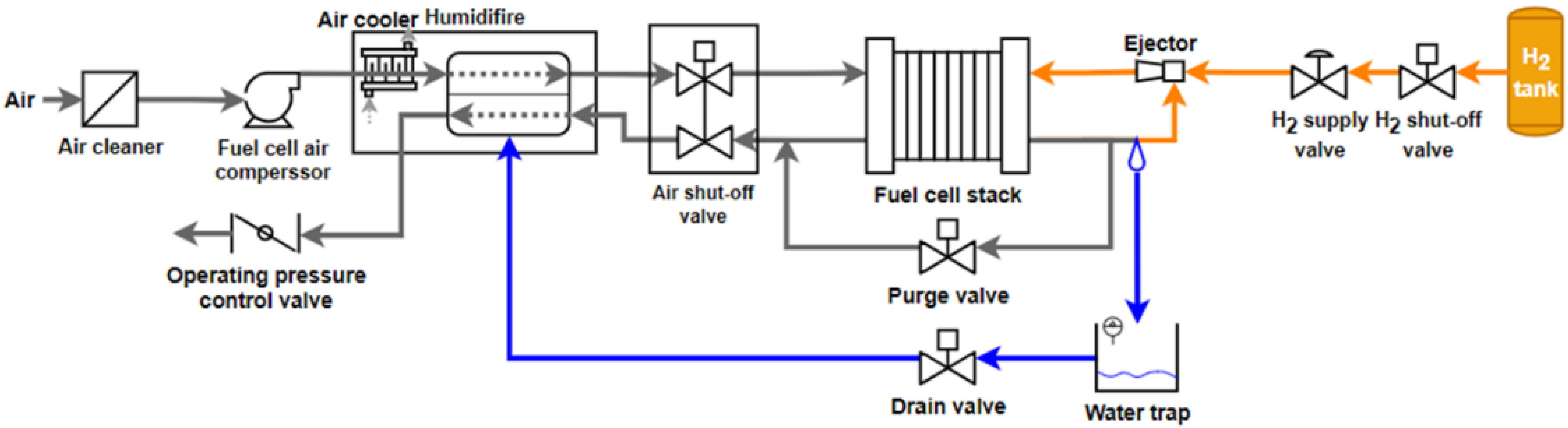

Fig. 1.2 Schematic diagram of PEM fuel cell TMS system

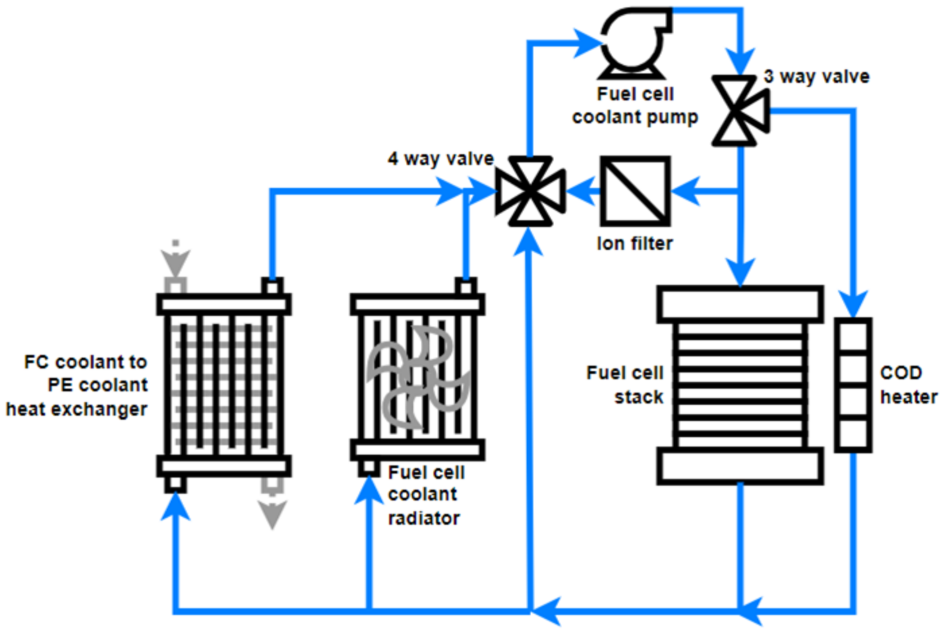

1.2. Literature review

The fuel cell technology has emerged as the predominant power source for fuel cell electric vehicles, presenting advantages such as high energy conversion efficiency, minimal noise, and remarkable reliability. The fuel cell power generation system, encompassing the fuel cell stack, is a sophisticated integrated system that spans across multiple disciplines, including electricity, thermodynamics, and electrochemistry. To enhance our comprehension of this system, researchers have established models using AMESIM and MATLAB Simulink for the PEM fuel cell system, enabling the analysis of fuel cell stack characteristics and its subsystems under dynamic conditions.

1.2.1 Modeling of PEM fuel cell BOP system

There were previous research papers that studied modeling of PEM fuel cell membrane humidifier and water balance [5,6,7,8,9,10]. Peng et al. [5] focused on studying a membrane humidifier that utilizes fuel cell exhaust gas to maintain proper membrane humidity in a PEM fuel cell system. A thermodynamic model was developed to capture essential dynamic variables of the humidifier, such as air flow pressure, flow rate, temperature, and relative humidity. Steady-state simulations were conducted to optimize the humidifier design, and dynamic simulations predict its behavior during transient operations seen in automotive applications. A proportional controller was designed to regulate the humidifier's operation. Choe et al. [6] introduced a mathematical model for the humidifier based on thermodynamic principles, analyzing heat and mass transfer as well as static and dynamic behaviors.

The model's accuracy was verified by comparing simulations with experimental data, and it was then used to study the effects of geometric parameters and operating conditions on performance. Additionally, step responses of the humidifier at different flow rates were analyzed. Proracki et al. [7] aimed to create a flexible computer-based simulation tool for designing planar humidifier systems. The simulation was based on mass transfer concepts and literature data on membrane behavior. The model assumed condensed liquid water on the humidifier membrane and accounted for a fraction of the membrane covered by liquid water while the rest was exposed to gaseous water concentrations. Several water coverage estimation models were derived and compared, but no single method was found to be universally superior. Mulyazmi et al. [8] investigated the water balance in the PEM fuel cell based on water transport phenomena. The diffusion of water from the cathode to the anode side was not observed at specific relative humidity levels, and the concentration of condensed water at the cathode side was minimal at certain operating conditions. On the anode side, water condensation was observed at specific operating temperatures. Tang et al. [9] investigated the water balance in the PEM fuel cell based on water transport phenomena. The diffusion of water from the cathode to the anode side was not observed at specific relative humidity levels, and the concentration of condensed water at the cathode side was minimal at certain operating conditions. On the anode side, water condensation was observed at specific operating temperatures. Hwang et al. [10] suggested simple static model developed to understand the physical phenomena of the membrane humidifier concerning geometric and operating parameters. The model was based on the concept of a shell and tube heat exchanger and can estimate mass transport through the membrane. The results emphasized the importance of wet gas humidity and membrane thickness as critical parameters for improving the humidifier's performance

In addition, there were previous research papers that studied modeling of PEM fuel cell air supply system [11,12]. Chen et al. [11] discussed the dynamic response of air supply systems in PEM fuel cells. It analyzed the factors that influence the response speed of voltage and current in fuel cell systems, and provided insights into the dynamic performance of air supply systems. The paper included a system model and simulation results, but did not discuss the influence of temperature, humidity, and other parameters on the dynamic performance of the system. Zhang et al. [12] used AMESim and MATLAB/Simulink to develop a PEM fuel cell system model and analyze the air supply system. The simulation showed that the centrifugal compressor operated narrowly near the surge line during the NEDC driving cycle, unlike internal combustion engines (ICE) applications. Coupling the CEM with an expander notably reduced parasitic power, especially at high output power levels.

There were previous research papers that studied modeling of PEM fuel cell TMS system [13]. Lee et al. [13] created to forecast performance changes in a PEM fuel cell under different operating conditions and understand how thermal management affects its performance. The system included a PEM fuel cell stack, air supply, fuel supply, and thermal management components, each modeled thermodynamically with design considerations. By considering ambient temperature and cooling system variations, the program predicted temperature and output fluctuations in the PEM fuel cell stack, enabling analysis of overall system performance changes caused by design variations.

1.2.2 Modeling of PEM fuel cell system

In addition, studies were conducted to modeling the PEM fuel cell system [14,15,16,17,18]. Kang et al. [14] studied dynamic model of a stationary PEM fuel cell system was created using Matlab/SIMULINK®. The model included the fuel processing system, fuel cell stack with coolant, humidifier with anode tail-gas oxidizer (ATO), and an enthalpy wheel for cathode air. It utilized a quasi-two-dimensional unit PEM fuel cell unit cell to simulate species dynamics, mass conservation equations, and energy balance, capturing details of MEA behavior like water transport. The model's predictions effectively match observed dynamic catalytic partial oxidation (CPO) temperature, voltage, and stack coolant outlet temperature. It proved to be a valuable tool for studying the impact of inlet conditions and developing control strategies to enhance system performance. Pukrushpan et al. [15] predicted performance changes in a polymer electrolyte membrane fuel cell under different operating conditions and interprets the influence of thermal management on the system. The system comprises a fuel cell stack, air supply, fuel supply, and thermal management components, each thermodynamically modeled with design considerations. By accounting for ambient temperature and cooling system variations, the program anticipated temperature and output fluctuations in the fuel cell stack, enabling predictive analysis of overall system performance in response to design variations. Kim et al. [16] examined the influence of the air supply system on the efficiency of PEM fuel cell systems. Using MATLAB/Simulink, researchers simulated automotive PEM fuel cell systems, specifically a low-pressure system with a turbo-blower, to analyze the impact of stack temperature and air stoichiometry on efficiency and parasitic power. They also compared the net system efficiency and parasitic power of the air supply system between low-pressure and high-pressure PEM fuel cell systems at the same net power conditions. The study's results guided the development of innovative operating strategies for fuel cell vehicles. Kim et al. [17] focused on creating simplified performance models for automotive PEM fuel cell systems. Using the MATLAB/Simulink environment, the PEM fuel cell stack and BOP components, such as the turbo blower, humidifier, and cooling circuit, was modeled. The efficiency and performance of the automotive PEM fuel cell system was analyzed under various operating conditions. The study aimed to provide valuable insights and contribute to the development of reliable simulation tools for automotive PEM fuel cell systems. Kim et al. [18] investigated the impact of operating conditions on the efficiency and PEM fuel cell systems. Using the MATLAB/Simulink platform, an automotive fuel cell system with a turbo-blower was studied. Sensitivity analyses on key parameters, such as stack temperature, cathode air stoichiometry, cathode pressure, and relative humidity, revealed that cathode pressure had the most significant effect on system efficiency. The study emphasized the importance of precise control over fuel cell operating conditions for the reliable operation of automotive PEM fuel cell systems.

In addition, studies were conducted to modeling the FCEB system [19]. Egardt et al. [19] presented a FCEB model based on the Van Hool FC bus equipped with a 150 kW PEM fuel cell. The main objective is to simulate the hydrogen consumption for the FCEB given a specific driving cycle. The research discussed the methodology, model structure, and calculation order, as well as the results of the simulation of hydrogen consumption for the fuel cell electric bus.

In the field of PEM fuel cell system modeling, several previous research studies have been conducted, focusing on various aspects of the system. Some of the key areas of prior research include:

1. Membrane Humidifier Modeling: Previous studies, such as those conducted by Peng et al. [5], Choe et al. [6], Proracki et al. [7], and Mulyazmi et al. [8], have addressed the modeling of membrane humidifiers in PEM fuel cell systems. These studies have explored different approaches to maintain proper membrane humidity and optimize the design of the humidifier. They have investigated various factors such as air flow pressure, flow rate, temperature, and relative humidity to improve the performance of the humidifier. However, despite these efforts, there may still be opportunities to further refine the modeling techniques and explore new ways to enhance the efficiency and reliability of the humidifier system.

2. Air Supply System Modeling: Researchers like Chen et al. [11] and Zhang et al. [12] have extensively studied the dynamic response of air supply systems in PEM fuel cells. These studies have provided valuable insights into the behavior of the air supply system and its impact on the overall performance of the fuel cell. However, some areas remain less explored, such as the influence of temperature, humidity, and other environmental parameters on the dynamic performance of the air supply system. Further research could focus on these aspects to better understand and optimize the system's response under varying operating conditions.

3. TMS (Thermal Management System) Modeling: Lee et al. [13] have made significant contributions to the modeling of PEM fuel cell TMS systems, enabling the prediction of performance changes under different operating conditions. However, there is still room for improvement in accurately modeling the complex heat and mass transfer phenomena within the TMS. Additional research could be directed toward developing more comprehensive and accurate models that consider factors like coolant flow rates, coolant temperatures, and ambient conditions to further optimize the thermal management and overall performance of the fuel cell stack.

In conclusion, while there have been notable advancements in PEM fuel cell modeling, there are areas where research is still lacking or where further improvements can be made.

1.3. Objective

The FCEBs equipped with fuel cells and batteries in a hybrid have recently been in the spotlight due to their eco-friendly and low-noise characteristics and their strengths in simplifying hydrogen charging and maintenance infrastructure. In addition, the high energy density value of hydrogen helps improve the vehicle's energy storage capacity and vehicle mileage, making it highly applicable to trucks, buses, and other means of transportation.

However, FCEBs frequently accelerate or decelerate depending on the driving route, and the load weight of FCEBs frequently changes depending on the number of bus passengers. Due to the nature of the FCEB, which frequently changes the demanded power, it adversely affects the durability of the fuel cell, and various studies are being conducted to solve this problem.

In the domain of PEM fuel cell system modeling research, prior investigations have primarily focused on individual components such as the humidifier, air supply system, and thermal management system (TMS). However, recognizing the significance of a holistic approach, this study embarked on a more comprehensive endeavor by developing a system-level model that encompasses the entire fuel cell electric bus (FCEB) PEM fuel cell system. This involved modeling not only the fuel cell stack but also the intricate balance of plant (BOP) system and the TMS.

To ensure the credibility and robustness of the model, a rigorous validation process was conducted. The simulation results were meticulously compared with real-world FCEB test data obtained through practical experiments. The aim was to scrutinize the agreement between the model predictions and the actual performance of the fuel cell system under various operating conditions, thereby demonstrating the accuracy and reliability of the developed model.

Through this comprehensive approach, in this study, the PEM fuel cell system constituting the PEM fuel cell stack, the air supply system, the hydrogen supply system, and the TMS were modeled. Referring to previous papers, modeling was conducted through physical phenomena and governing equations for each component and integrated into the system model using Simcenter AMESIM®. As a result, the PEM fuel cell system model was verified by comparison with vehicle experimental data.

Chapter 2. Model descriptions

2.1 Modeling of PEM fuel cell unit cell

2.1.1 Model development

The PEM fuel cell is an electrolyte membrane-electrode assembly (MEA) that enables hydrogen ion exchange. It consists of a gas diffusion layer (GDL) that facilitates the diffusion of the reactive gas into the catalyst layer and the discharge of water generated after the reaction, and a bipolar plate (BP) that acts as a flow path for the reactive gas. The schematic diagram PEM fuel cell unit cell is shown with the Fig. 2.1. The developed model considers the diffusion of reactant gases in the GDL and the catalyst layer (CL), as well as the impact of water within the fuel cell stack. It takes into account the oxygen concentration in the gas channels and the CL, and models the transport processes considering changes in the mass transfer coefficients and water transport equations in the MEA under different operating conditions (temperature, pressure, relative humidity). Furthermore, the model utilizes experimental data from polarization curves to determine the values of the constants used in the model.

Fig. 2.1 Schematic diagram of PEM fuel cell unit cell

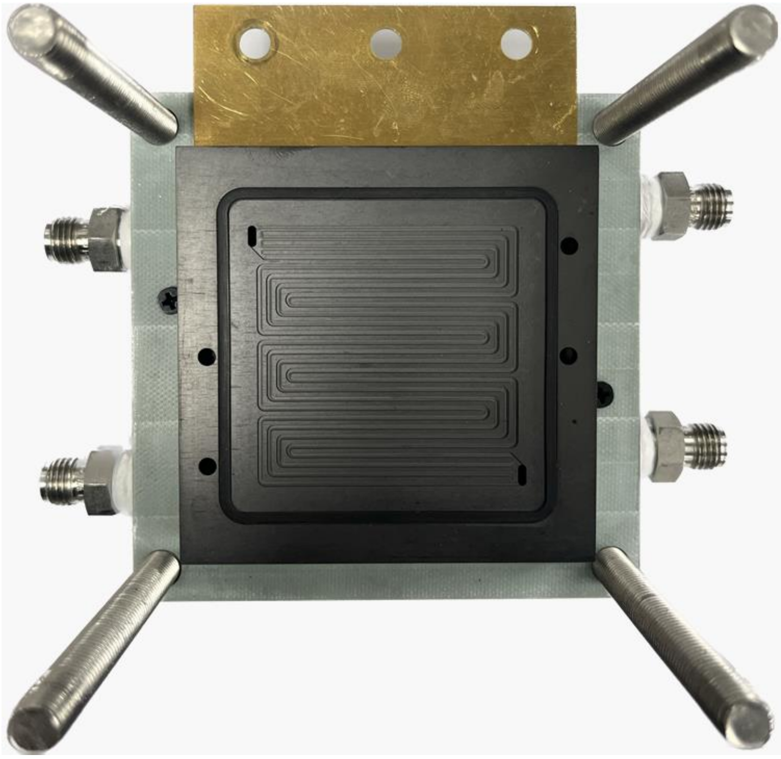

2.1.2 Electrochemical equations

Water generated by electrochemical reaction in the cathode catalyst layer of PEM fuel cell generates three internal resistances. Internal resistances include activation loss due to kinetics at the electrode, ohmic loss representing ionic and electron resistance, and concentration loss representing change in reactant concentration at platinum. The empirical formula was applied to AMESIM so that resistance values according to the ion conductivity and current density of the membrane could be calculated through electrochemical equations. The voltage of fuel cell is calculated by subtracting the three voltage losses from the Nernst voltage with Eq. (2.1) [14].

$$\mathrm{V} = V_{nernst} - V_{act} - V_{ohm} - V_{cons} \tag{2.1}$$

Where V_{nernst} is the PEM fuel cell unit cell Nernst voltage. It is the open circuit voltage of a single cell of the PEM fuel cell stack. The cell voltage would reach this value, if the whole Gibbs free energy of reaction is converted into electrical energy. Activation, ohmic and concentration overpotentials are responsible of the decrease in voltage. U_{act} is the cell activation voltage drop, U_{ohm} is the cell ohmic voltage drop, and U_{cons} is the cell concentration voltage drop.

The activation voltage loss is the simplified form of Butler-Volmer equation used as an activation energy loss for electrochemical reactions in PEM fuel cell with Eqs. (2.2), and (2.3) [19].

$$V_{act} = \frac{R \cdot T}{\alpha \cdot n \cdot F} \log\left(\frac{(j_{stack} + j_n)}{j_0}\right) \tag{2.2}$$

$$j_0 = j_0^{ref} \cdot \left(\frac{C_{O_2c}}{C_{O_2c,ref}}\right)^{\gamma} \cdot e^{\frac{-E_{O_2}}{RT}\left(1 - \frac{T}{T_0}\right)} \tag{2.3}$$

Where R is the gas constant (8.3145 [J/mol/K]), T is the temperature of the stack[K], n is the number of electrons involved in the reaction, here n = 2, F is the Faraday's constant (96485.3415 [C/mol]), α is the charge transfer coefficient, j_{stack} is the stack current density [mA/cm^2], j_n is the internal current density [mA/cm^2], and j_0 is the exchange current density [mA/cm^2]. The j_0 is calculated with the O_2 concentration at the cathode C_{O_2c} [mol/m^3] and on the stack temperature T [K].

The ohmic voltage loss is a resistance loss, which is influenced by the proton conductivity of the membrane, as the current increases, the resistance increases as the charge moves more with Eqs. (2.4), (2.5), and (2.6) [19].

$$V_{ohm} = R_{memb} \cdot j'_{stack} \tag{2.4}$$

$$R_{memb} = \frac{l_{memb}}{\sigma_{memb}} \tag{2.5}$$

$$\sigma_{memb} = \left(0.005139 \cdot \lambda_{H_2O} - 0.00326\right) \cdot exp\left(1268\left(\frac{1}{298} - \frac{1}{T}\right)\right) \tag{2.6}$$

Where R_{memb} is the membrane proton area specific resistance (also called membrane ohmic resistance) [Ohm $\cdot$ cm^2], j'_{stack} is the current in the stack [A/cm^2], σ_{memb} is the membrane proton conductivity [S/cm], l_{memb} is the membrane thickness [cm], and λ_{H_2O} is the water content in the membrane.

The concentration voltage loss is affected by the limit current density value due to the voltage loss caused by insufficient hydrogen gas supply for the electrochemical reaction of the PEM fuel cell with Eq. (2.7) [19].

$$V_{cons} = -B \log\left(1 - \frac{j_{stack}}{j_l}\right) \tag{2.7}$$

Where B is the concentration voltage drop coefficient [V], j_{stack} is the current density in the stack [mA/cm^2], and j_l is the limiting current density [mA/cm^2].

2.1.3 Water transport

PEM fuel cell generates water and heat by electrochemical reactions, and both cations and anions are generated by catalysts and must move in the electrolyte, so water is required and it is important to apply it to fuel cell unit cell modeling.

In a wet electrolyte, the movement of hydrogen ions is at its peak, while in a dry electrolyte, hydrogen ions are unable to migrate due to the absence of separated sulfone bonds. On the other hand, when water is generated and swells in the water passage and the pores of the electrode, it overflows and blocks gas diffusion. This also makes the output current non-uniform and causes the current density to drop, so to improve the performance of the fuel cell, an appropriate equilibrium must be maintained between the drying and overflow of the electrolyte membrane. The amount of water is calculated using the activity value of water and the amount of water in the membrane is calculated using the average value of the amount of water in the cathode and anode side with Eqs. (2.8), and (2.9) [8].

$$\boldsymbol{\lambda_{H_2O}} = \frac{\boldsymbol{\lambda_{H_2O_c}+\lambda_{H_2O_a}}}{\boldsymbol{2}} \tag{2.8}$$

$$\lambda_{H_2O_j}\begin{cases} 0.043 + 17.81aH_2O_j - 39.85\left(aH_2O_j\right)^2 + 36\left(aH_2O_j\right)^3 & if \quad aH_2O_j \le 1 \\ 14 + 1.4\left(aH_2O_j - 1\right) & if \quad 1 < aH_2O_j \le 3 \\ 16.8 & if \quad 3 < aH_2O_j \end{cases} \tag{2.9}$$

Where λ_{H_2O} is the water content in the membrane, $\lambda_{H_2O_c}$ is the water content in the membrane at the cathode side, $\lambda_{H_2O_a}$ is the water content in the membrane at the anode side, and aH_2O_j is the H_2O activity at electrode.

Water is produced by oxygen reduction reactions. As a result, the concentration of water is higher on the cathode side than on the anode side, and due to the difference in concentration, water diffuses from the cathode to the anode, which is called back diffusion and calculated with Eqs. (2.10), (2.11), (2.12), and (2.13) [8].

$$dn_{H_2O_{Diff}} = D_{Diff} \cdot \frac{C_{H_2O_c} - C_{H_2O_a}}{l_{memb}} \cdot N_{cell} \cdot S_{cell} \tag{2.10}$$

$$C_{H_2O_j} = \lambda_{H_2O_j} \cdot \frac{\rho_{memb}}{EW} \tag{2.11}$$

$$D_{Diff} = D_0 \cdot k_{corr(T)} \tag{2.12}$$

$$k_{corr(T)} = exp\left(2416\left(\frac{1}{T_0} - \frac{1}{T_{cell}}\right)\right) \tag{2.13}$$

Where D_{Diff} is the H_2O diffusion coefficient in membrane $[m^2/s]$, $C_{H_2O_j}$ is the H_2O concentration in membrane at electrode $[\mathrm{mol}/m^3]$, l_{memb} is the membrane thickness [m], S_{cell} is the PEM fuel cell unit cell active area $[m^2]$, N_{cell} is the number of cells in the stack, $\lambda_{H_2O_j}$ is the water content at electrode, ρ_{memb} is the dry membrane density $[\mathrm{kg}/m^3]$, and EW is the dry membrane equivalent weight $[\mathrm{kg/mol}]$. It is the dry polymer weight per mole of acid group. D_0 is the diffusion coefficient $[m^2/s]$ depending on water content λ_{H_2O} of the membrane, $k_{corr(T)}$ is the correction factor according to the stack temperature, and T_0 is the reference temperature.

On the other hand, hydrogen ions are moved from the anode to the cathode by an electric field, and the surrounding water molecules are also dragged along, which is called electro-osmosis drag and calculated with Eqs. (2.14), and (2.15) [8].

$$\boldsymbol{dn_{H_2O_{eo}} = n_{drag} \cdot \frac{I_{stack}}{F} \cdot N_{cell}} \tag{2.14}$$

$$\boldsymbol{n_{drag} = \frac{2.5}{22} \cdot \lambda_{H_2O}} \tag{2.15}$$

Where $dn_{H_2O_{eo}}$ is the H_2O molar flow rate due to electro-osmosis $[\mathrm{mol/s}]$, and n_{drag} is the electro-osmosis drag coefficient which is calculated with membrane water content λ_{H_2O} and on the stack temperature T. I_{stack} is the output stack current [A]

Water equilibrium was applied to the fuel cell unit cell model by applying empirical formulas such as water content and concentration values according to temperature that could simulate water flow phenomena occurring within the fuel cell unit cell.

2.2 Modeling of PEM fuel cell stack

The stack was modeled by stacking unit fuel cells to produce demanded power. The schematic diagram of PEM fuel cell stack is shown with the Fig. 2.2. The voltage and current for generating the demanded power is calculated through the Eq. (2.16) [19]. The characteristics of the j-V curve vary depending on the temperature and relative humidity of the stack. The FCEB j-V curve is shown in the Fig. 2.3 from the results of the dynamometer FCEB vehicle test data.

$$P_{dmd} = V_{out} I_{out} = n_{cell} P_{cell} = n_{cell} V_{cell} I_{out} \tag{2.16}$$

The molar flow rate of the gas reacted in the stack and the generated water were calculated using the Faraday's constant (F=96,458 C/mol) as follows with Eqs. (2.17) [8].

$$\dot{N}_{H_2,re} = \frac{n_{cell} I_{out}}{2F}$$

$$\dot{N}_{O_2,re} = \frac{n_{cell} I_{out}}{4F}$$

$$\dot{N}_{Air,re} = \frac{1}{0.21} \frac{n_{cell} I_{out}}{4F}$$

$$\dot{N}_{H_2O,pro} = \frac{n_{cell} I_{out}}{2F} \tag{2.17}$$

The mass flow rate of fuel to be supplied to cathode and anode is calculated as follows with Eqs. (2.18) [8], considering the molar mass and the stoichiometry ratio (SR) of each gas.

$$\frac{\dot{N}_{H_2,in}}{\dot{N}_{H_2,re}} = \lambda_{H_2}$$

$$\frac{\dot{N}_{O_2,in}}{\dot{N}_{O_2,re}} = \frac{\dot{N}_{Air,in}}{\dot{N}_{Air,re}} = \lambda_{Air} \qquad (2.18)$$

The PEM fuel cell stack simulation model is modeled using PEM fuel cell unit cell simulation model, and the modeling mechanism is shown in Fig. 2.4.

Fig. 2.2 Schematic diagram of FCEB PEM fuel cell stack

Fig. 2.3 Cell voltage vs. current density of FCEB PEM fuel cell

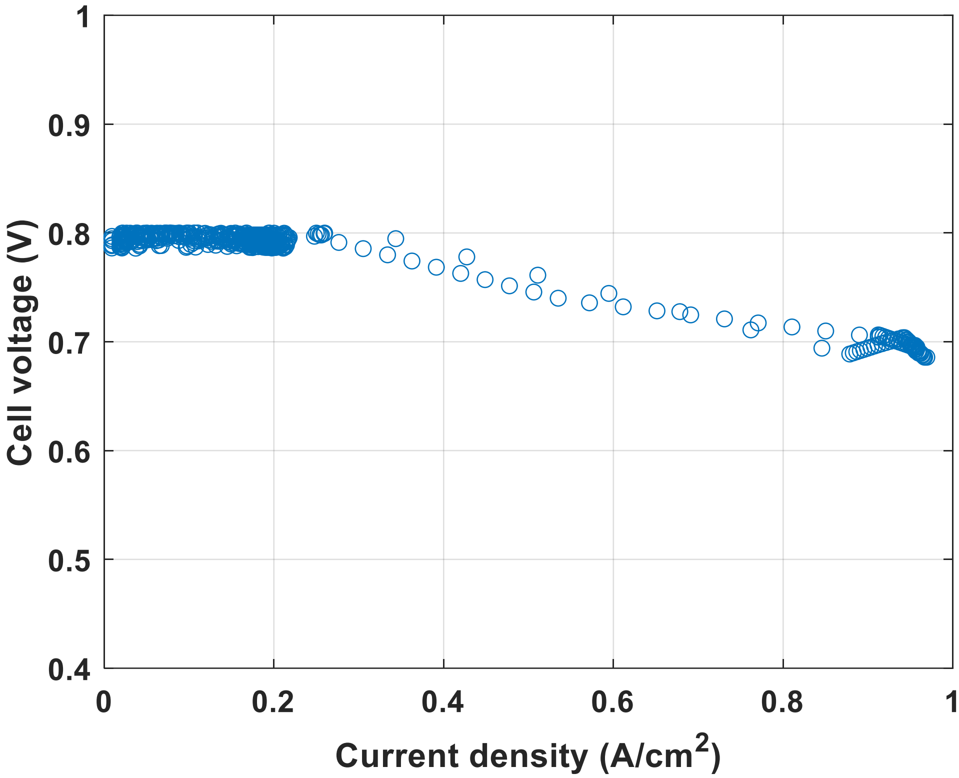

Fig. 2.4 Schematic diagram of PEM fuel cell stack AMESIM simulation model

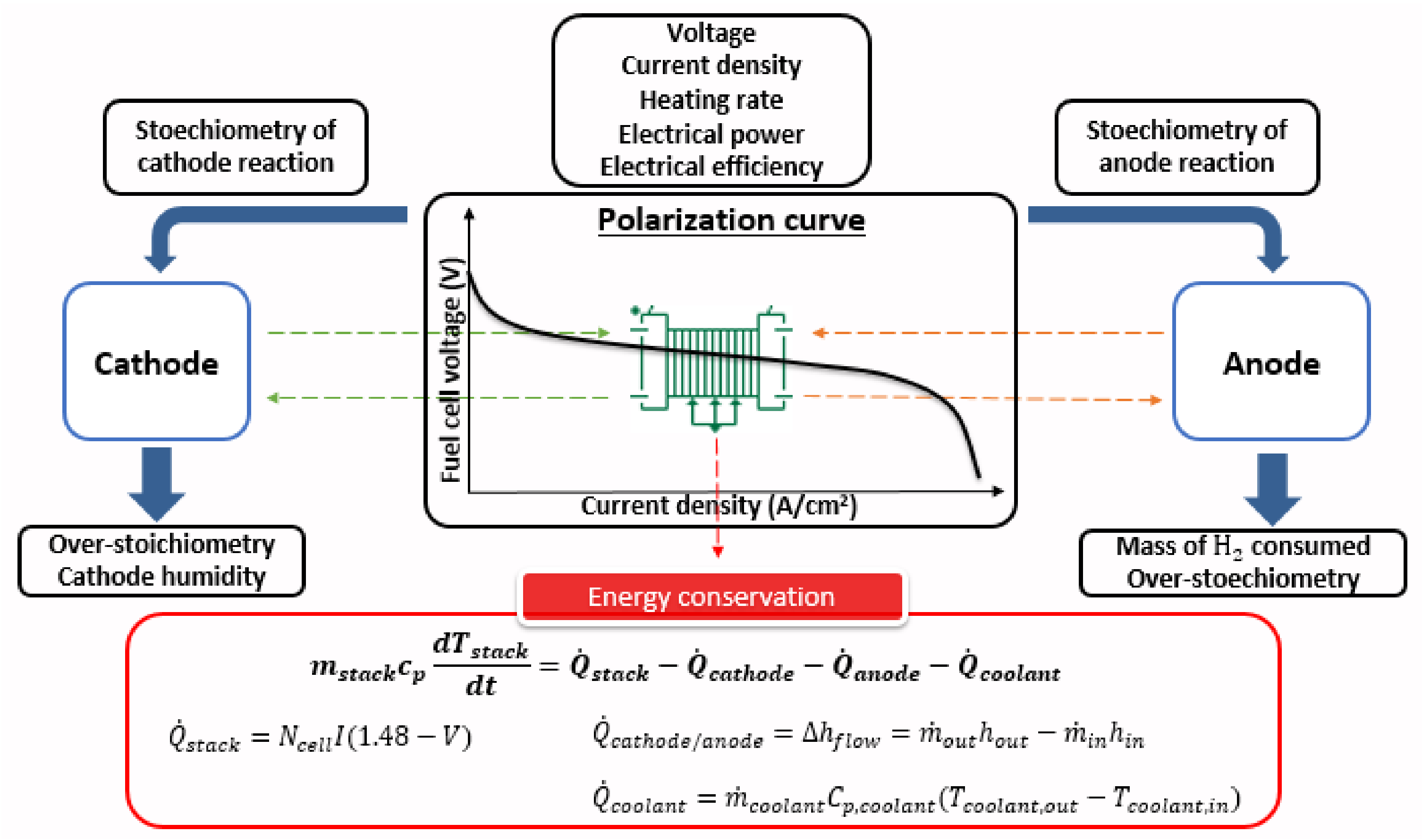

2.3. Modeling of membrane humidifier

2.3.1 Model development

The fuel cell air supply system is shown with Fig. 2.6. The water molecule transport due to the concentration gradient between the shell and tube through the membrane control volumes is calculated by the following empirical equation with Eq. (2.19) [5,21].

$$\frac{dm_{H_2O}}{dt} = D_w \frac{C_2 - C_1}{t_m} M_v A \tag{2.19}$$

Where M_v is the vapor molar mass, C_1 and C_2 represent water concentrations in control volumes 1 and 2, respectively. The membrane coefficient of diffusion, D_w is determined by the following empirical equation with Eq. (2.20) [5,21].

$$D_w = D_\lambda e^{2416(1/303 - 1/T_m)} \tag{2.20}$$

Where T_m is the membrane temperature. The coefficient D_λ is determined empirically and has a piecewise-linear form with Eq. (2.21) [5,21].

$$D_\lambda = \begin{cases} 10^{-6} & \lambda_m < 2 \\ 10^{-6}\left(1 + 2(\lambda_m - 2)\right) & 2 \le \lambda_m \le 3 \\ 10^{-6}\left(3 - 1.67(\lambda_m - 3)\right) & 3 < \lambda_m < 4.5 \\ 1.25 * 10^{-6} & \lambda_m \ge 4.5 \end{cases} \tag{2.21}$$

Where λ_m is the membrane water content which will be defined in following equation with Eq. (2.23) [5]. The water concentration of both Channel is calculated with Eq. (2.22) [5].

$$C = \frac{\rho_m}{M_m} \cdot \lambda \tag{2.22}$$

$$\lambda = \begin{cases} 0.043 + 17.81a - 39.85a^2 + 36a^3 & for\ \ 0 < a \le 1 \\ 14 + 1.4(a - 1) & for\ \ 1 < a \le 3 \end{cases} \tag{2.23}$$

Where ρ_m is the dry membrane density, M_m is the dry membrane equivalent weight, and λ is the membrane water content.

2.3.2 Water drain

In the case of the cathode outlet, the relative humidity exceeds 100% due to the water generated by the fuel cell power generation, and the condensed water is discharged to the outside through the water trap and drain valve. The amount of water drained in this way is calculated through the following calculation formula with Eq. (2.24) [8].

$$\text{Relative humidity}, \Phi = \frac{P_{water\ vapor}}{P_{sat}} = \frac{\dot{N}_{water\ vapor}}{\dot{N}_{sat}}$$

$$\text{In case of } \Phi > 1, \dot{N}_{sat} = \frac{\dot{N}_{water}}{\Phi}$$

$$\dot{N}_{water,liquid} = \dot{N}_{water} - \dot{N}_{sat} = \dot{N}_{water}\left(1 - \frac{1}{\Phi}\right)$$

$$\dot{m}_{water,liquid} = M_{H_2O}\dot{N}_{water,liquid} \qquad (2.24)$$

$\dot{N}_{water}$ is calculated as the sum of the amount of water entering the stack cathode and the amount of water produced by the electrochemical reaction in the stack with Eq. (2.25) [8].

$$\dot{N}_{water} = \dot{N}_{cathode,in} + \dot{N}_{gen}$$

$$\dot{N}_{gen} = \frac{N_{cell} \cdot I}{n \cdot F} \qquad (2.25)$$

2.3.3 Energy conservation

The energy conservation law is used to determine the temperature of the entire humidifier, and convective heat transfer with residual air and moisture in the cathode outlet is calculated using Newton's cooling law with Eqs. (2.26), and (2.27) [5].

$$NC_V \frac{dT}{dt} = \sum \dot{N}_{in} h_{in} - \sum \dot{N}_{out} h_{out} + \sum \dot{Q}_{in} \tag{2.26}$$

$$\dot{Q} = A \cdot h \cdot (T_2 - T_1) \tag{2.27}$$

Where h is the convective heat transfer coefficient and is set as a constant value. The schematic diagram of PEM fuel cell membrane humidifier is shown with the Fig. 2.5. The membrane humidifier AMESIM simulation model is shown in Fig. 2.7.

Fig. 2.5 Schematic diagram of FCEB membrane humidifier

Fig. 2.6 Schematic diagram of PEM fuel cell air supply system

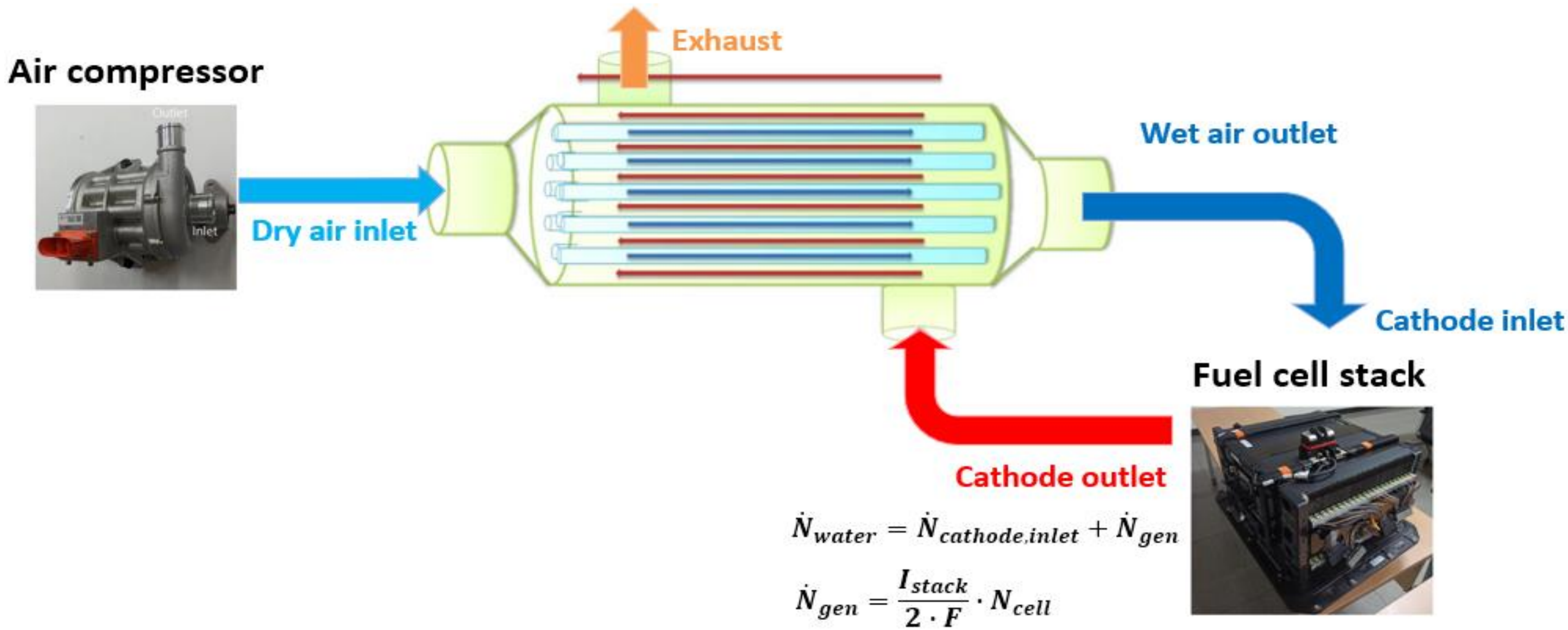

Fig. 2.7 Schematic diagram of membrane humidifier AMESIM simulation model

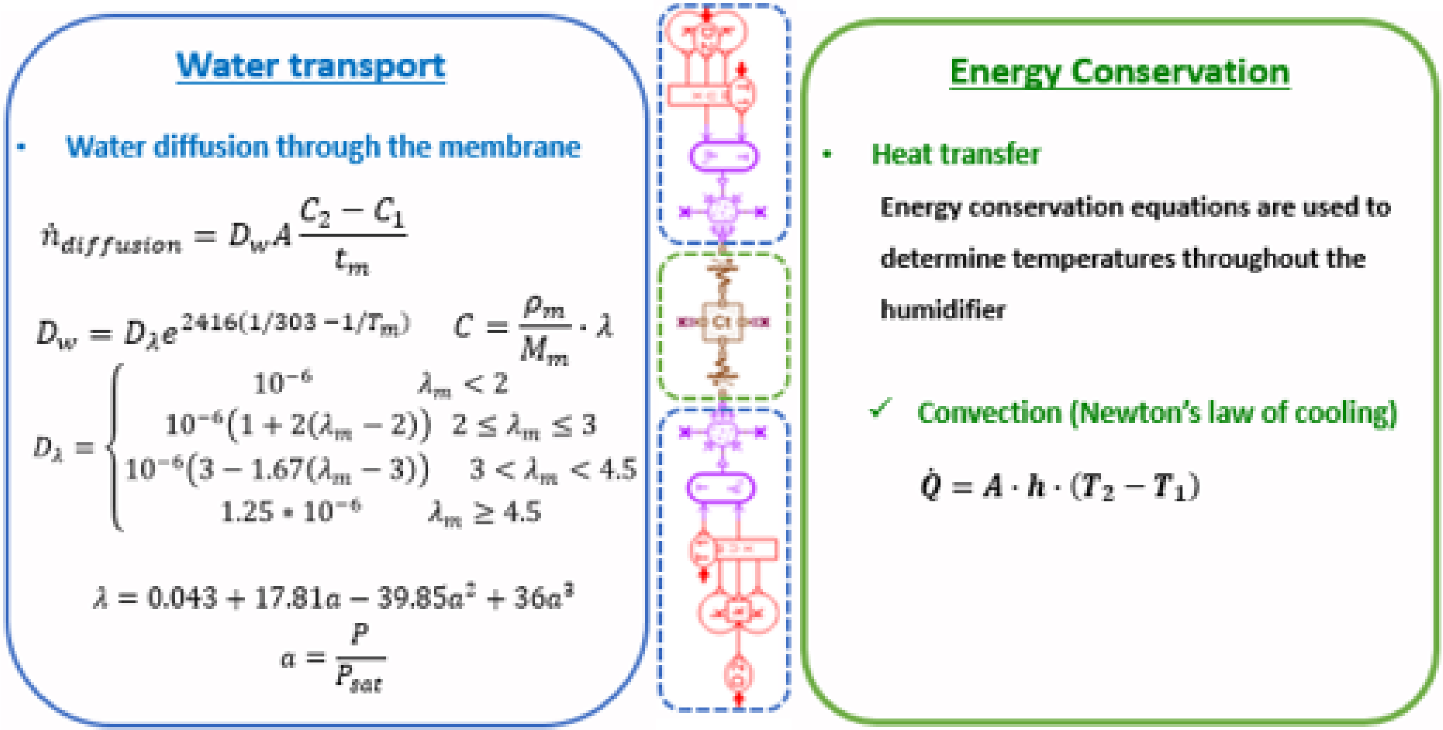

2.4 Modeling of air compressor

2.4.1 Model development

The air compressor used in FCEB is a centrifugal compressor type. A centrifugal compressor is a type of dynamic compressor used to compress gases, including air and various process gases. It operates on the principle of utilizing centrifugal force to increase the gas's kinetic energy, followed by converting this kinetic energy into pressure energy. The schematic diagram of air compressor is shown with the Fig. 2.8.

The air compressor includes a compression unit such as an impeller/volt and a high-speed motor unit for driving the compression unit, and is a device for supplying air required for a reaction of a fuel cell stack at an appropriate flow rate/pressure. The flow rate is controlled according to the number of rotations of the motor, and the induced air is compressed by the high-speed rotation of the impeller connected to the motor shaft. The air compressor is modeled with the inlet/outlet pressure ratio and isentropic efficiency tested at the reference temperature and pressure as the corrected flow rate and the corrected rotational speed of the air compressor [22,23]. Pressure ratio and isentropic efficiency are calculated with Eqs. (2.28), and (2.29) [22,23]. The air flow rate during the operation of the compressor is proportional to the speed of the compressor, and the air flow rate according to the pressure change inlet and outlet the compressor is shown in Fig. 2.9. The isentropic efficiency is shown in Fig. 2.10 from the results of the dynamometer FCEB vehicle test data.

$$Pr_{ac} = \frac{p_{ac,out}}{p_{ac,in}} = f(\dot{m}_c, \dot{\omega}_c) \tag{2.28}$$

$$\eta_{ac} = \frac{T_{ac,out}^{is} - T_{ac,in}}{T_{ac,out}^{real} - T_{ac,in}} = f(\dot{m}_c, \dot{\omega}_c) \tag{2.29}$$

Where $\dot{m}_c$ is the corrected mass flow rate, $\dot{\omega}_c$ is the corrected rotational speed of the air compressor, $T_{ac,out}^{is}$ is the isentropic temperature, $T_{ac,out}^{real}$ is the real temperature, $p_{ac,out}$ is the pressure of air compressor outlet, and $T_{ac,in}$ and $p_{ac,in}$ are temperature and pressure of air compressor inlet respectively

Fig. 2.8 Schematic diagram of FCEB air compressor

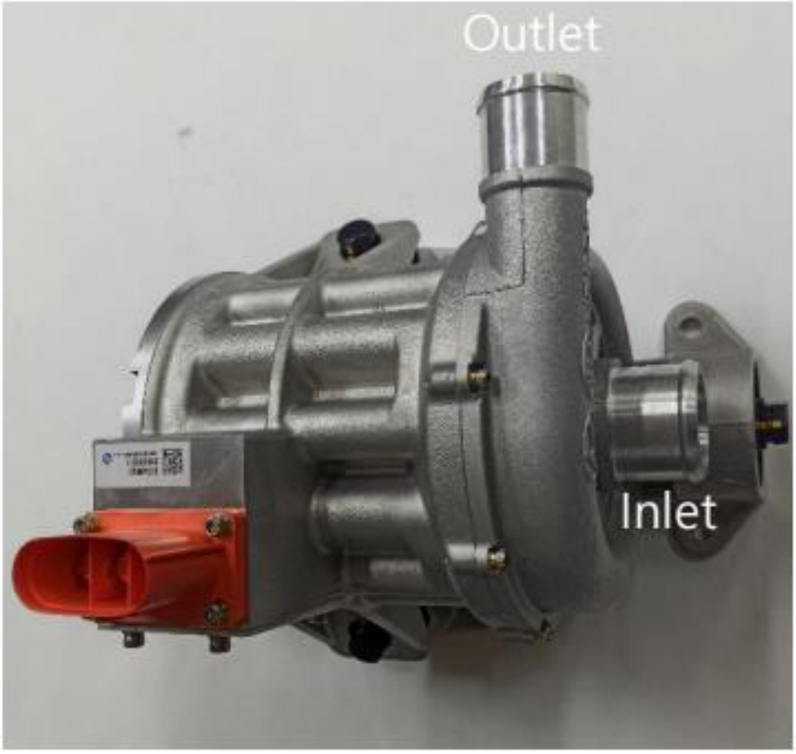

Fig. 2.9 Air compressor pressure ratio according to corrected mass flow rate ($\dot{m}_c$) and air compressor speed ($\dot{\omega}_c$)

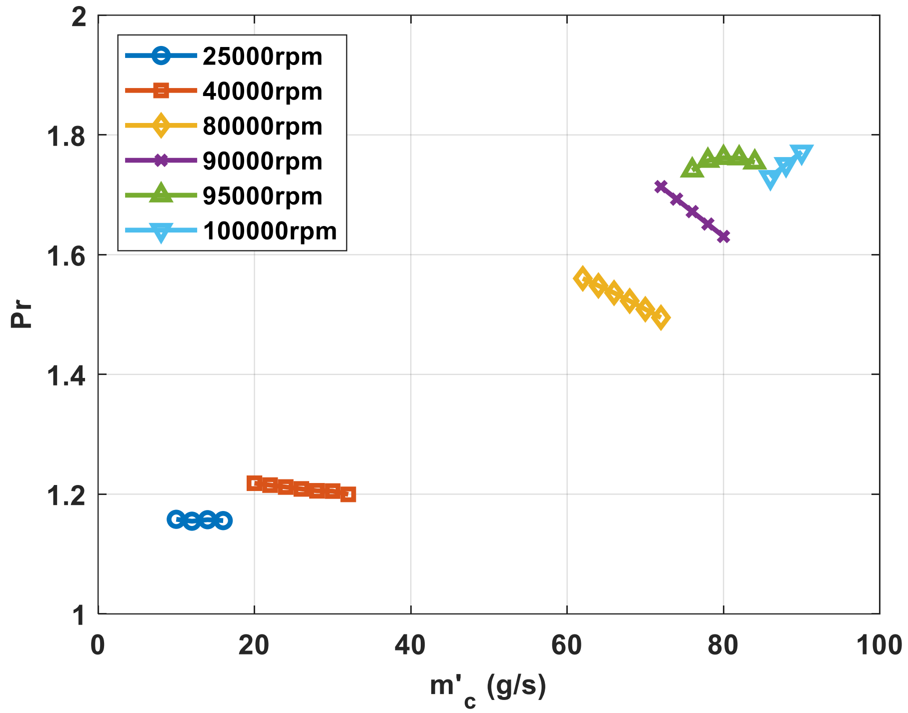

Fig. 2.10 Air compressor isentropic efficiency according to air compressor outlet isentropic temperature ($T_{ac,out}^{is}$) and real temperature ($T_{ac,out}^{real}$)

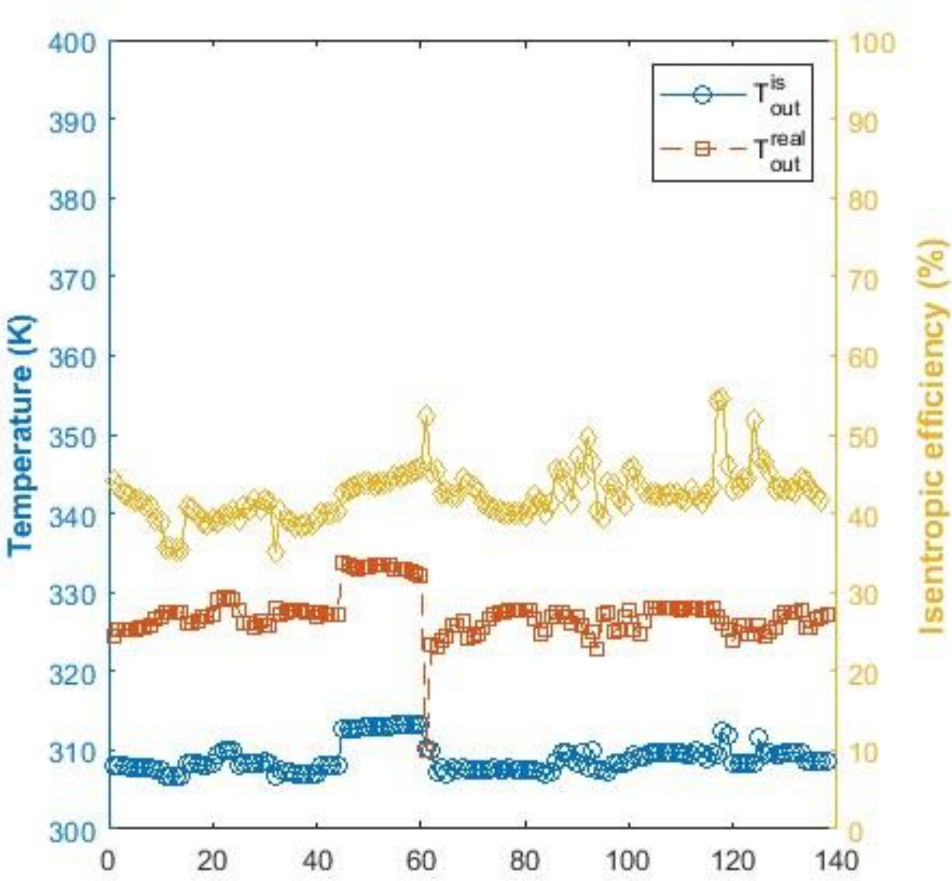

2.4.2 Operating pressure control valve

The operating pressure control valve is a component that adjusts the opening of the valve according to the outside air condition so that the stack is pressurized. The schematic diagram of operating pressure control valve is shown with the Fig. 2.11. It is adjusted through the relationship between the valve cross-sectional area and the operating pressure according to the flow rate, flow coefficient, fluid temperature, and valve opening through the operating pressure regulator as following Eq. (2.30) [24].

$$\dot{m}_{opcv} = A_{opcv} \cdot C_{q,opcv} \cdot C_{m,opcv} \cdot \frac{p_{opcv,in}}{\sqrt{T_{opcv,in}}} \tag{2.30}$$

Where A_{opcv} is the restriction area $[m^2]$, $C_{q,opcv}$ is the flow coefficient, $C_{m,opcv}$ is the mass flow parameter $[\sqrt{kg \cdot K/J}]$, $p_{opcv,in}$ is the upstream pressure [PaA], and $T_{opcv,in}$ is the upstream temperature.

Fig. 2.11 Schematic diagram of FCEB operating pressure control valve

2.5 Modeling of Thermal Management System

2.5.1 Coolant pump

The coolant pump model calculates coolant flow rate and a power consumption according to operation of the coolant pump. The volume flow rate map or reference data according to the pressure drop in the coolant circuit and the number of revolutions of the coolant pump are used. When the reference data is used, the affinity law of centrifugal pump is used to obtain the flow rate and power consumption. The affinity law is as follows with Eqs. (2.31) [25].

$$\dot{Q} = \frac{\dot{Q}_{ref} N D^3}{N_{ref} D_{ref}^3} = \frac{\dot{Q}_{ref} N D^3}{C_q}$$

$$\mathrm{p} = \frac{\rho p_{ref} (ND)^2}{\rho_{ref} (N_{ref} D_{ref})^2} = \frac{\rho p_{ref} (ND)^2}{C_p}$$

$$\mathrm{P} = \frac{\rho P_{ref} N^3 D^5}{\rho_{ref} N_{ref}^3 D_{ref}^5} = \frac{\rho P_{ref} N^3 D^5}{C_W} \tag{2.31}$$

Where N is the reference rotary speed, D the reference pump diameter, and ρ the reference fluid density.

2.5.2 Radiator

The FCEB's stack cooling system consists of a pump, a fan, and a radiator, and is one of the most power-consuming parts of the BOP in the cooling system. The role of the oil pump in the cooling system is forced heat exchange through a radiator, so the corresponding parts are indicated as a radiator in the model.

The radiator was modeled so that the results could be derived from a 2D table of air velocity through the fan, coolant flow rate through the radiator, and how much heat must be dissipated through the radiator.

The air velocity passing through the radiator is calculated by considering the velocity of incoming air from the outside and the velocity of incoming air due to the rotation of the radiator fan with Eq. (2.32) [26].

$$V_{air} = V_{drive} + V_{fan} \tag{2.32}$$

Where V_{air} is the air velocity through the radiator, V_{drive} is the velocity of incoming air from the outside, and V_{fan} is the velocity of incoming air due to the rotation of the radiator fan.

In the case of FCEBs, unlike general passenger cars, the radiator is located on the side of the vehicle, so it is judged that the effect of air inflow caused by vehicle speed is extremely small. The radiator fan velocity is calculated with Eq. (2.33) [26].

$$V_{air} = V_{drive} + V_{fan} = V_{fan} \tag{2.33}$$

$(\because V_{drive} \approx 0)$

The air flow rate passing through the radiator fan is as follows with Eq. (2.34) [26].

$$\dot{m}_{fan} = \rho V_{fan} A_{fan} \tag{2.34}$$

Where ρ is air density, and A_{fan} is radiator fan area

The external environment and the initial conditions of the stack are assumed to be normal, and the outer and inner diameters of the radiator fan is calculated using the measured values.

The temperature change of the stack is affected by the difference between the heating value of the stack and the amount of heat taken by fluids such as coolant, hydrogen, and air passing through the stack. The PEM fuel cell stack temperature is determined by Eqs. (2.35) [20].

$$m_{stack} c_p \frac{dT_{stack}}{dt} = \dot{Q}_{stack} - \dot{Q}_{cathode} - \dot{Q}_{anode} - \dot{Q}_{coolant}$$

$$\dot{Q}_{stack} = N_{cell} \cdot I(E^H - V)$$

$$\dot{Q}_{cathode/anode} = \Delta h_{flow} = \dot{m}_{out} h_{out} - \dot{m}_{in} h_{in}$$

$$\dot{Q}_{coolant} = \dot{m}_{coolant} C_{p,coolant} \left(T_{coolant,out} - T_{coolant,in}\right) \tag{2.35}$$

Where $\dot{Q}$ is the heat flux, c_p the specific heat of the material at temperature T, and E^H is the reversible open circuit voltage.

The amount of heat that the coolant passing through the stack exchanges with the stack is an important control factor for controlling the temperature of the stack, which is calculated from the following Eqs. (2.36) [20]. The heat transfer coefficient is affected by the Nusselt number. The Nusselt number is calculated with Reynolds number and Prandtl number.

$$\dot{Q}_{cool} = hA(T_{stack} - T_{FCcool,stack,\,in})$$

$$h = \frac{Nu \cdot k_f}{D_H}$$

$$Nu = 1.86 Re^{1/3} Pr^{1/3} \left(\frac{D}{L}\right)^{1/3} \left(\frac{\mu_b}{\mu_w}\right)^{0.14} \tag{2.36}$$

Where D_H is the hydraulic diameter [mm], k_f is the fluid conduction heat transfer coefficient [W/m · k], Nu is the Nusselt number, Re is the Reynolds number, Pr is the Prandtl number, $\frac{D}{L}$ is the ratio of the tube length, diameter. and $\frac{\mu_b}{\mu_w}$ is the ratio of bulk and wall viscosity.

2.6 Fuel Cell Electric Bus

The fuel cell electric buses (FCEBs) are a distinct category of electric buses that stand apart from conventional electric buses. They generate electricity using fuel cells instead of relying on rechargeable electric batteries. FCEBs are increasingly recognized as an efficient and eco-friendly solution for future public transportation. They incorporate lightweight batteries and significantly reduce fuel charging time.

Figs. 1.1 and 1.2 illustrate the process of fuel supply for generating electric energy within the fuel cell system of the FCEB and the configuration of the TMS responsible for controlling stack temperature, respectively. Air is supplied to the cathode end of the fuel cell stack through a compressor, with a pressure control valve at the humidifier outlet for efficient regulation. At the anode end, high-pressure hydrogen is introduced from the hydrogen tank through a pressure control valve, and any unused hydrogen is effectively recycled via an ejector.

Thermal management of the fuel cell stack is achieved by using coolant, which flows through channels between the stack separators. This aspect ensures excellent electrical insulation and corrosion prevention within the fuel cell stack. The integrated FCEB system, combining the fuel cell and battery, is represented in Fig. 2.12.

The calculation of the demanded driving power takes into account driving conditions and the efficiency of the driving motor. It also includes the energy required for thermal management and the activation of various actuators within the

BOP system. Separate assessments are conducted to determine the demanded power of the fuel cell and battery, respectively.

The demanded power includes the power consumption of the Fuel Cell BOP system, TMS system, and battery TMS system. The FC BOP system's power consumption is related to the energy required for supplying fuel from the BOP to meet the stack's power demand. On the other hand, the power consumption of the TMS system is attributed to managing the heat generated during power generation, and this energy supply comes from both the stack and the battery. All these factors are carefully considered in the comprehensive computation of the total power demand, as depicted in Fig. 2.13.

The method of calculating the demanded power is shown in the following Eqs. (2.37), and (2.38) [19].

$$P_{dmd} = P_{motor,in} + P_{others} = P_{stack,out} + P_{batt,out} \tag{2.37}$$

$$P_{others} = P_{stack,BOP} + P_{stack,TMS} + P_{batt,TMS} + P_{loss} \tag{2.38}$$

Where P_{dmd} is the demanded power of FCEB, $P_{motor,in}$ is the motor output power, $P_{stack,out}$ and $P_{batt,out}$ are the PEM fuel cell stack and battery output power respectively, and P_{others} is the FCEB BOP system including PEM fuel cell BOP, TMS and battery TMS power consumption.

Fig. 2.12 Schematic diagram of FCEB system

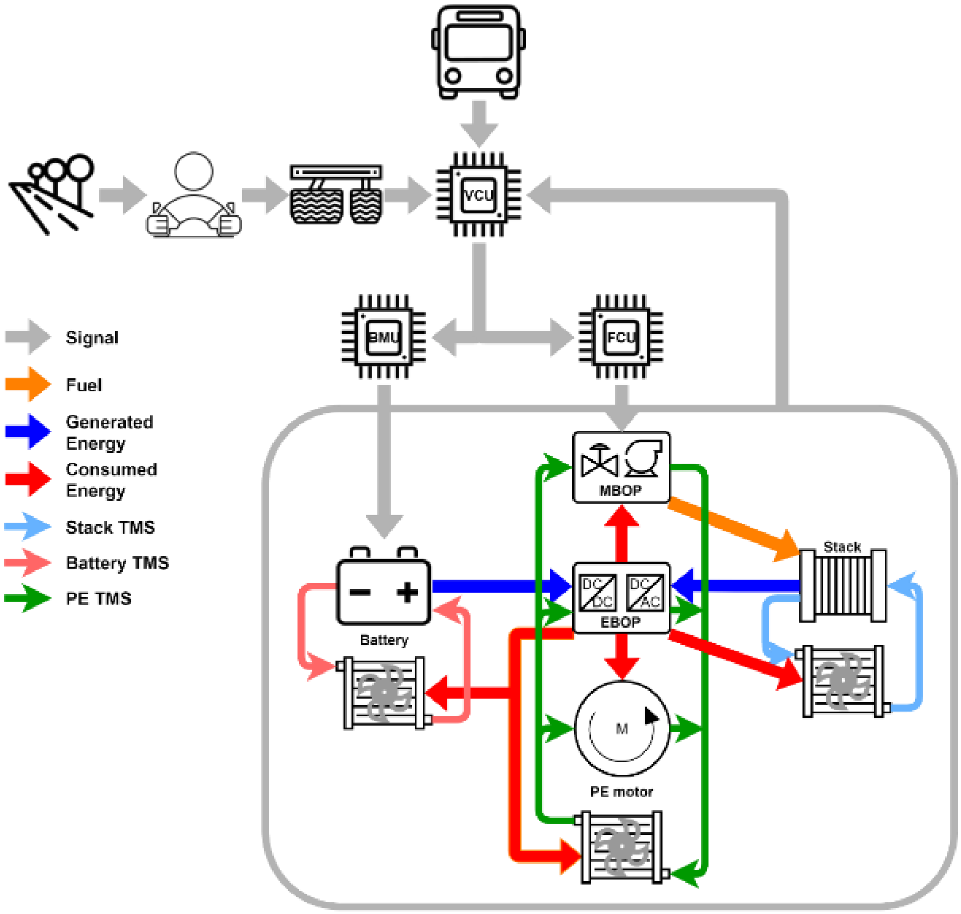

Fig. 2.13 Schematic diagram of FCEB demanded power calculation method

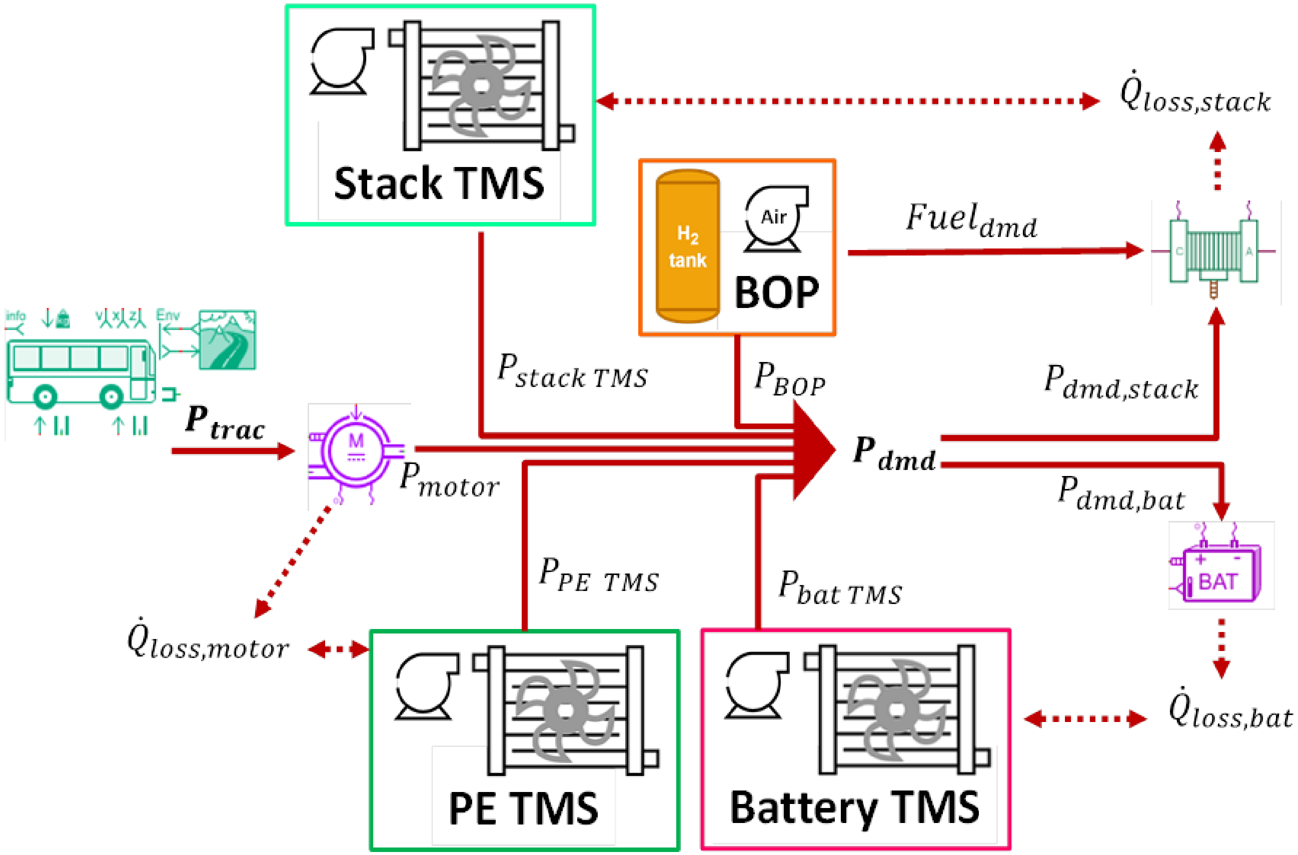

2.7 FCEB system energy flow

There are various devices that use power in this fuel cell system. These BOP systems use power from high-voltage battery packs, but also use some of the power generated from the fuel cell stack for component with a high level of power consumption. This is a loss of fuel cell stack power and must be considered essential when conducting a test to check the specifications of the fuel cell stack. Therefore, it is important to understand the level of power consumed by each BOP system, and this will be analyzed through dynamometer vehicle tests and modeling.

Fig. 2.14 shows the overall power distribution system for FCEB. The overall energy flow during bus driving was analyzed through dynamometer vehicle test and modeling results. Two fuel cell stack, air compressor, and coolant pump are used in the vehicle system. However, according to the test results, the two parts do not always have the same power value, but for convenience of calculation, it is assumed that the same parts produce the same power.

The total power in the FCEB system may be expressed as the sum of the fuel cell stack power and the battery power. In addition, the sum of the two powers is equal to the sum of the powers consumed by the bus's drive motor and other BOP systems. In this equation, the efficiency of motor is assumed to be 90%. The demanded power of FCEB is determined by Eq. (2.39) [19].

After conducting dynamometer vehicle tests, the power consumed by each BOP system was measured using a current, voltage sensor, which is shown in Figs. 2.15, 2.16, and 2.17, respectively. Based on the test results, the power consumed in each

BOP system was trended in a relational expression according to the fuel cell stack power and temperature. In the case of air compressor, the power required by the stack tends to be proportional to the air compressor's operating speed, so the trend line for stack power appears as shown in Fig. 2.15 below. The power consumption of component is calculated with Eqs. (2.40), (2.41), and (2.42), respectively. Based on the stack power results, three sections that is determined as a relatively steady state were found, and the energy flow from the corresponding power is calculated with power and power consumption value.

$$P_{dmd} = P_{motor,in} + P_{others} = P_{stack,out} + P_{batt,out} \tag{2.39}$$

$$P_{aircomp} = 0.0009 \times P_{stack}^2 - 0.0088 \times P_{stack} + 0.3808 \tag{2.40}$$

$$P_{oilpump} = 8 \times 10^{-7} \times T_{stack}^6 - 0.0003 \times T_{stack}^5 + 0.035 \times T_{stack}^4$$

$$-2.5 \times T_{stack}^3 - 100.7 \times T_{stack}^2 - 2136.3 \times T_{stack} + 18795 \tag{2.41}$$

$$P_{coolpump} = -9 \times 10^{-8} \times T_{stack}^6 + 3 \times 10^{-5} \times T_{stack}^5 - 0.004 \times T_{stack}^4$$
$$+0.29 \times T_{stack}^3 - 11.9 \times T_{stack}^2 + 257.5 \times T_{stack} - 2315.6 \tag{2.42}$$

Where $P_{aircomp}$, $P_{oilpump}$, and $P_{coolpump}$ are power consumption of air compressor, oil pump of radiator, and coolant pump respectively, and P_{stack} and T_{stack} are the power and temperature of PEM fuel cell stack respectively.

Fig. 2.14 Schematic diagram of FCEB electrical BOP

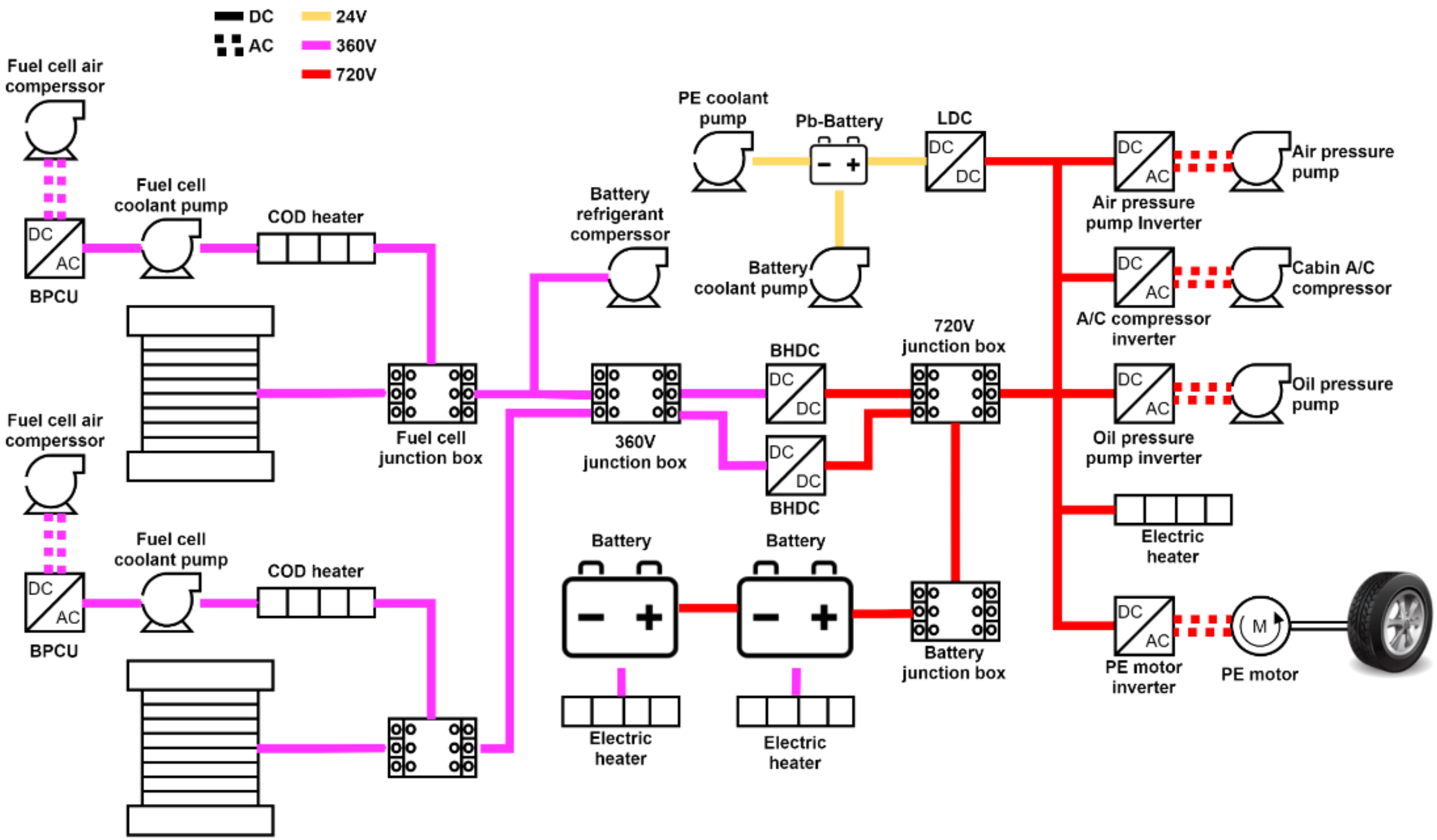

Fig. 2.15 Power consumption of air compressor according to PEM fuel cell stack power

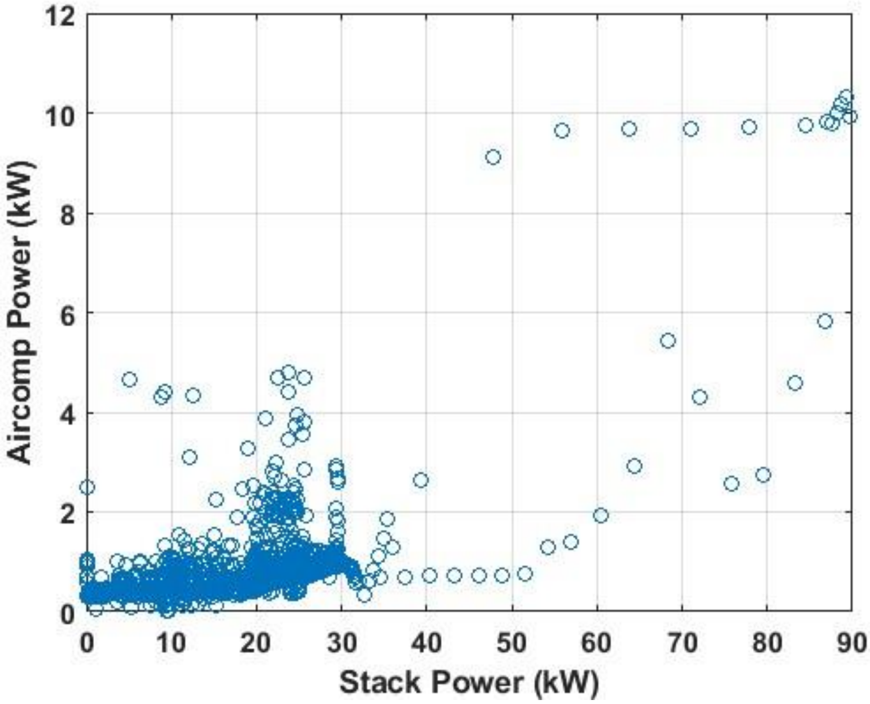

As the output power of the PEM fuel cell stack increases, there is a corresponding increase in the demand for oxygen supply to support the electrochemical reactions within the fuel cell. The air compressor plays a crucial role in providing the required amount of air (oxygen) to the fuel cell stack. Therefore, with an increase in the stack output power, the air compressor needs to operate at a higher capacity to deliver an adequate and continuous flow of air.

Consequently, the power consumption of the air compressor tends to rise proportionally with the increasing power output of the PEM fuel cell stack. This relationship is due to the direct correlation between the power requirement of the air compressor and the stack's power demand for efficient and optimal operation of the fuel cell system.

In summary, as the output power of the PEM fuel cell stack rises, the air compressor's power consumption also increases, ensuring a sufficient supply of air to sustain the fuel cell's electrochemical reactions and overall system performance.

Fig. 2.16 Power consumption of coolant pump according to PEM fuel cell stack temperature

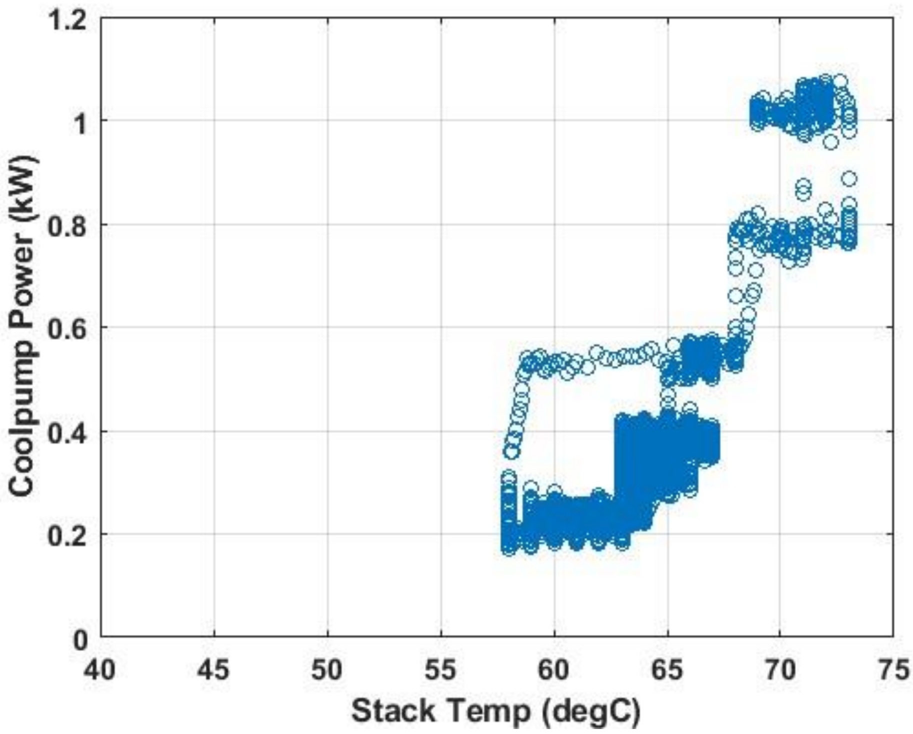

When the stack operates at a higher temperature, it generates more heat due to increased electrochemical reactions. To maintain the stack within the desired temperature range and ensure optimal performance, the coolant pump needs to work harder to circulate a larger volume of coolant to dissipate the excess heat.

As a result, the power consumption of the coolant pump tends to increase with higher operating temperatures of the PEM fuel cell stack. This relationship is due to the increased cooling demand and the need for more energy to circulate the coolant effectively.

On the other hand, when the stack operates at a lower temperature, it generates less heat, and the cooling demand on the coolant pump decreases. Consequently, the power consumption of the coolant pump reduces, as it requires less energy to circulate a smaller volume of coolant to maintain the stack at the appropriate temperature.

In summary, the power consumption of the coolant pump in a PEM fuel cell system is directly related to the operating temperature of the fuel cell stack. Higher stack temperatures lead to increased cooling demand and higher power consumption of the coolant pump, while lower stack temperatures result in reduced cooling demand and lower power consumption of the pump, ensuring efficient thermal management and optimal operation of the fuel cell system.

Fig. 2.17 Power consumption of oil pump radiator according to PEM fuel cell stack temperature

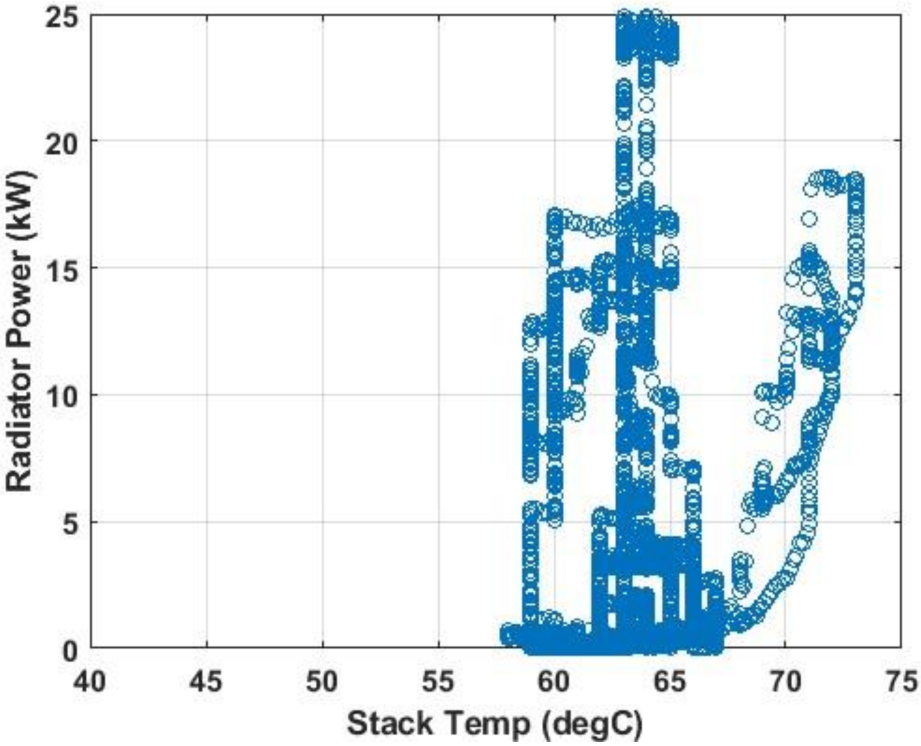

In a PEM fuel cell system, the oil pump for the radiator is responsible for circulating the cooling oil to dissipate the excess heat generated by the fuel cell stack during its operation. When the stack operates at a higher temperature, it produces more heat due to increased electrochemical reactions. As a result, the cooling system requires more energy to circulate a larger volume of cooling oil to effectively remove the excess heat from the stack and maintain it within the desired temperature range.

Therefore, with an increase in the operating temperature of the PEM fuel cell stack, the power consumption of the oil pump for the radiator tends to rise. This relationship is due to the increased cooling demand and the need for additional energy to circulate the cooling oil efficiently.

Conversely, when the stack operates at a lower temperature, it generates less heat, and the cooling demand on the radiator's oil pump decreases. As a result, the power consumption of the oil pump reduces, as it requires less energy to circulate a smaller volume of cooling oil to maintain the stack at the appropriate temperature.

In summary, the power consumption of the oil pump for the radiator in a PEM fuel cell system is directly related to the operating temperature of the fuel cell stack. Higher stack temperatures lead to increased cooling demand and higher power consumption of the oil pump, while lower stack temperatures result in reduced cooling demand and lower power consumption of the pump, ensuring efficient thermal management and optimal operation of the fuel cell system.

Chapter 3. Simulation results and discussion

3.1 Verification of PEM fuel cell unit cell model

The simulation simulated operation with flow rate of cathodes SR 2.0 and anode SR 1.5 in Galvanostatic technique test mode. The performance test conditions were shown in Table 3.1. The specifications of the fuel cell unit cell and various operating conditions were simulated with Table 3.2.

Table. 3.1 Performance test conditions

Parameter	Test conditions
Test mode	Galvanostatic technique
Mass flow	Anode : SR 1.5 Cathode : SR 2.0
Reactant gas	H_2 / Air

Table. 3.2 Operation conditions

Parameter	Operation conditions
Cell temperature [℃]	55, 65, 75
Relative humidity [%]	50, 70, 100
Outlet pressure [bar]	1, 1.5, 2.0 (absolute pressure)

In this study, the activation overpotential was induced from the Tafel equation, and the exchange current density was expressed as a function of oxygen concentration, including concentration losses. The charge transfer coefficient's values were determined by fitting experimental data from a specific driving condition. Likewise, for the Ohmic losses, the ion conductivity was represented as a linear function of water content and an exponential function of temperature. The saturation level of liquid water in the GDL was also considered and incorporated into the model. The model's performance was then evaluated by comparing its predictions with experimental results from other driving conditions, demonstrating a good agreement between them.

The verification through the fuel cell unit cell simulation model and experimental value showed that the result value was followed well within 1% error with Figs. 3.1, 3.2, and 3.3. The figure displays the simulation results of a PEM fuel cell unit cell model, represented by the symbol. The solid line graph represents the experimental data of the PEM fuel cell unit cell.

Fig. 3.1 Simulation result of PEM fuel cell unit cell verification with I-V curve at various temperature conditions

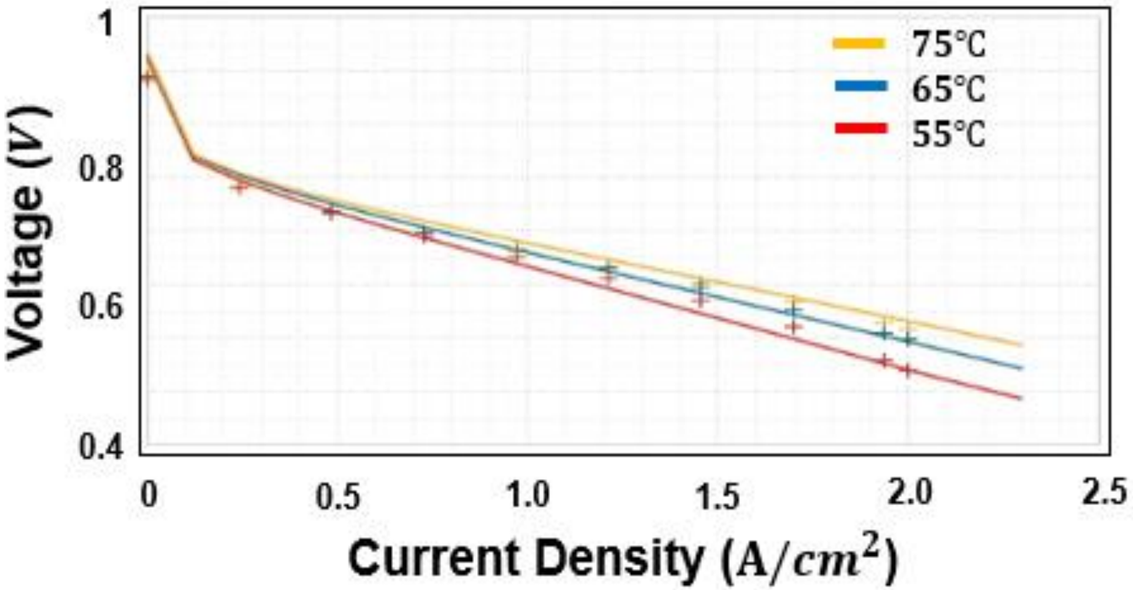

Temperature significantly impacts the PEM fuel cell polarization curve. Lower temperatures increase activation overpotential and ohmic losses, leading to decreased performance. In contrast, higher temperatures reduce these losses and enhance mass transport and water management, resulting in improved fuel cell efficiency and performance.

Fig. 3.2 Simulation result of PEM fuel cell unit cell verification with I-V curve at various pressure conditions

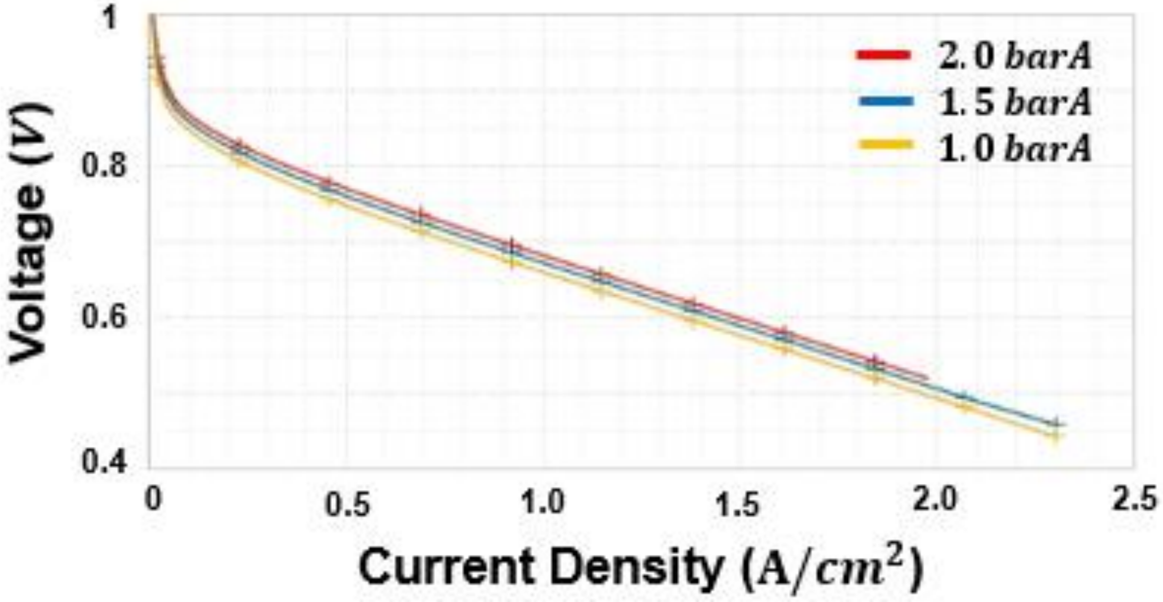

Higher pressure enhances reactant transport, leading to reduced concentration polarization and improved performance. Elevated pressure also decreases activation overpotential, resulting in higher cell voltage output. However, excessively high pressure may increase parasitic losses and stack complexity, affecting overall efficiency. Optimal pressure levels are crucial for achieving efficient and reliable PEM fuel cell operation.

Fig. 3.3 Simulation result of PEM fuel cell unit cell verification with I-V curve at various relative humidity conditions

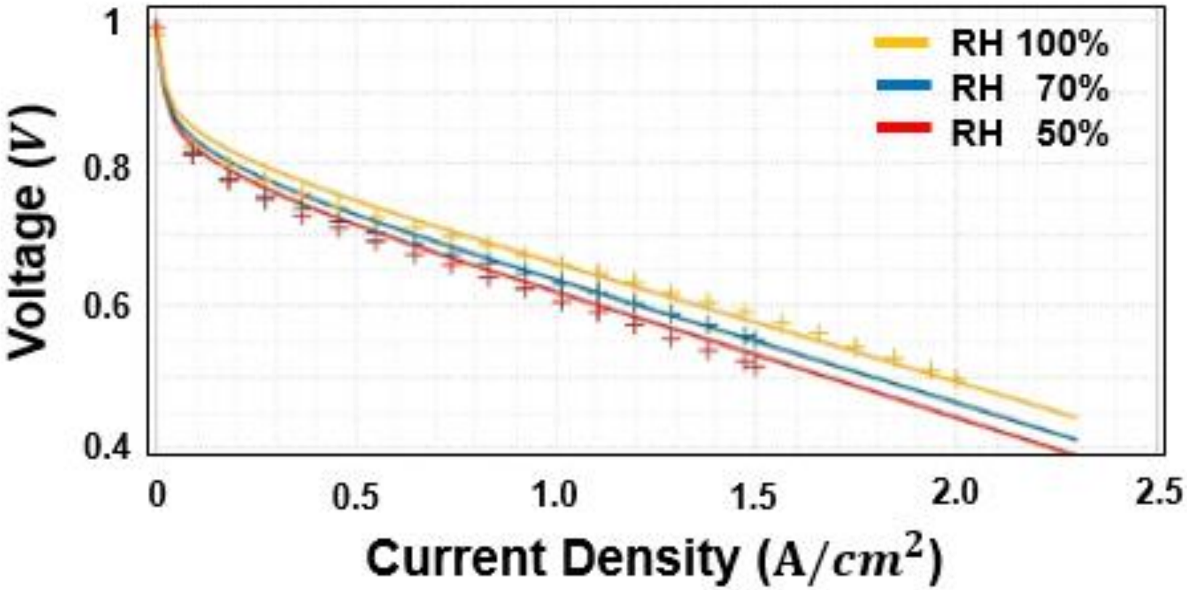

Higher relative humidity levels promote better water management, preventing reactant flooding and improving overall performance. Increased humidity enhances proton conductivity in the electrolyte, reducing activation and ohmic losses, leading to higher cell voltage output. However, excessively high humidity cause flooding and hinder reactant diffusion, increasing concentration polarization and decreasing cell efficiency. Maintaining an optimal relative humidity level is crucial for achieving efficient and stable PEM fuel cell operation.

3.2 Verification of PEM fuel cell stack model

The PEM fuel cell stack model was developed by stacking the modeled PEM fuel cell unit cells based on the number and area of PEM fuel cell unit cells used in the FCEB. The specifications of the PEM fuel cell stack are found in Table 3.3. The modeling process involved applying the same electrochemical equations and relationships for water transport that were used in the individual PEM fuel cell unit cell modeling.

Each PEM fuel cell unit cell was modeled using relevant electrochemical equations and equations for water transport to accurately represent its behavior. These individual unit cell models were then stacked together in the PEM fuel cell stack model to simulate the collective behavior of the entire stack in the FCEB. By utilizing the appropriate equations and relationships, the stack model was able to predict the performance and behavior of the PEM fuel cell stack under real-world operating conditions in the FCEB.

Table. 3.3 Specification of PEM fuel cell stack

Parameter	Value
Number of cells [$-$]	436
Cell area [cm^2]	30×11
Mass of stack [kg]	69.7

Fig. 3.4 Verification model PEM fuel cell stack power

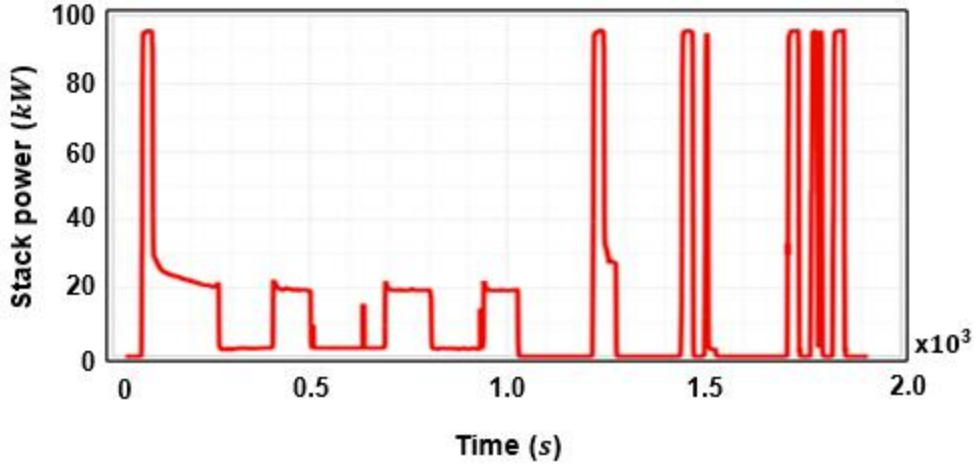

Fig. 3.5 Verification model PEM fuel cell stack I-V curve

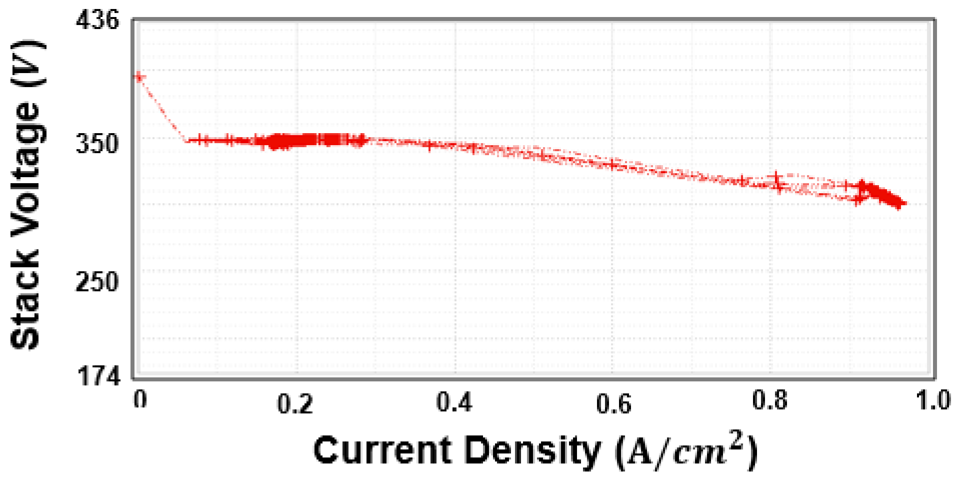

To validate the proposed PEM fuel cell stack model, the simulation results were compared with the transient data from FCEB dynamometer vehicle tests. Figs. 3.4 and 3.5 display the stack power and the polarization curve of the verified model stack, respectively.

Fig. 3.6 Simulation result of PEM fuel cell unit cell verification with I-V curve

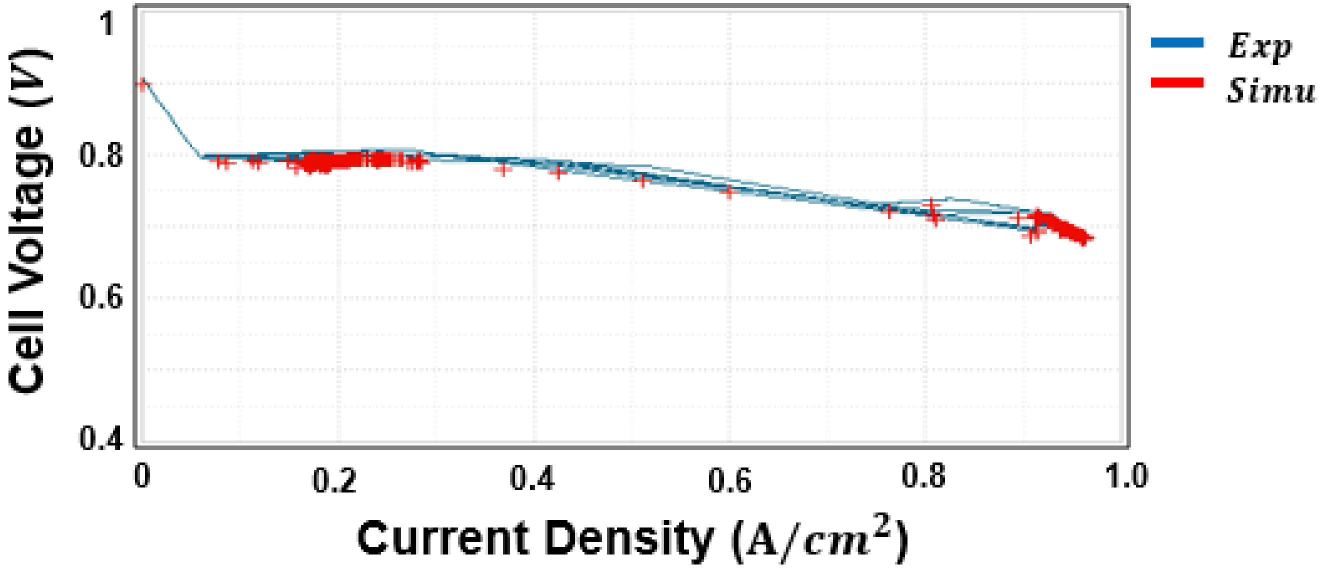

The simulation model of the PEM fuel cell stack is compared with the results of polarization curve of FCEB dynamometer vehicle test results. As illustrated in Fig. 3.6, it is evident that the experimental and simulation results matched very closely, with an error within 2%. However, as the current density approached 1 A/cm^2, some differences began to appear, which were attributed to the nonlinearity of the stack. In the experiments, the stack's temperature increased as the operation continued, causing the experimental results to deviate from the simulation results of the proposed model with fixed parameters. In other words, the fuel cell stack becomes more active as the temperature rises beyond 1 A/cm^2 with a rated power, reflecting the temperature characteristics of increasing the reversible open circuit voltage and slightly reducing the loss.

3.3 Verification of air compressor model

The air compressor is accurately modeled by incorporating several crucial parameters, including the inlet/outlet pressure ratio and isentropic efficiency data. These essential metrics are derived from meticulously conducted tests performed at standard reference temperature and pressure conditions. Additionally, the corrected flow rate and rotational speed of the air compressor are integrated into the model to ensure its precision and reliability.

To establish the model's credibility and authenticity, extensive validation efforts are undertaken. The data collected from dynamometer vehicle tests of the air compressor used in the FCEB play a pivotal role in this validation process. By comparing the model's predictions with the real-world results from the vehicle tests, the air compressor's behavior in various operating conditions and scenarios is verified. This comprehensive validation approach ensures that the air compressor model is a robust and effective tool for simulating and analyzing the performance of the entire fuel cell system.

Fig. 3.7 Simulation result of air compressor pressure ratio in steady state according to the corrected mass flow rate

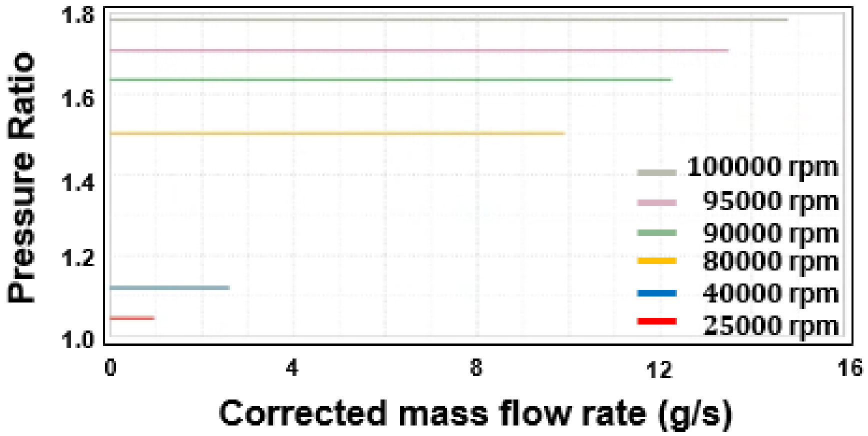

Fig. 3.8 Simulation result of SR

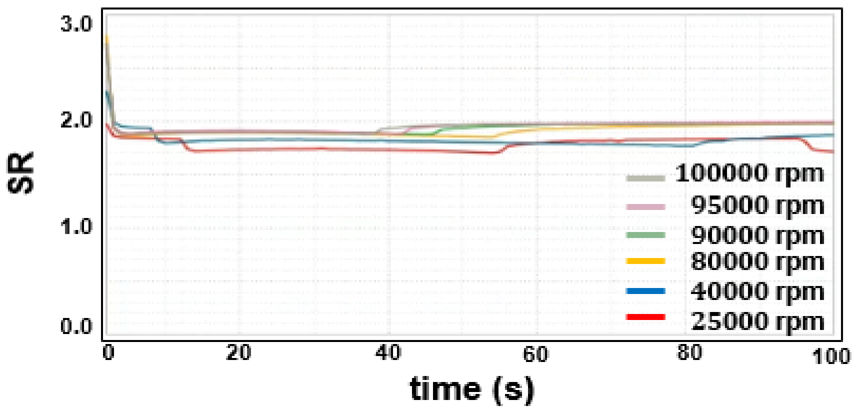

During the model verification process, comprehensive analysis by comparing the model's performance across a wide range of operating conditions were conducted. This involved examining different flow rates, air compressor inlet/outlet pressures, and temperature variations corresponding to the rotation speed of the FCEB air compressor.

The results of the air compressor verification in steady-state conditions, as depicted in Fig. 3.7, were highly promising. The corrected mass flow rate and pressure ratio data, obtained based on the rotational speed of the air compressor, exhibited a remarkably low error rate, well within the range of 1%. This outcome attested to the accuracy and reliability of our model in accurately predicting the air compressor's behavior under various operating scenarios.

Moreover, the operating pressure control valve is modeled to maintain a specific set point, known as the SR, at a value of 2.0. The flow rate supplied by the control valve was diligently regulated to ensure that the SR remained constant, and the throttle angle of the control valve was precisely adjusted to achieve this desired SR value. The simulation results depicting the SR's performance are presented in Fig. 3.8, demonstrating the effectiveness of our model in simulating the pressure control valve's functionality with a high degree of accuracy.

Overall, the rigorous model verification process and subsequent simulation results reaffirm the robustness and suitability of our approach in capturing the complex dynamics of the air compressor and pressure control valve, crucial components of the FCEB's fuel cell system. These findings not only validate the model but also provide valuable insights for optimizing the performance and efficiency of the fuel cell system in real-world applications.

Fig. 3.9 Simulation result of air compressor corrected mass flow rate

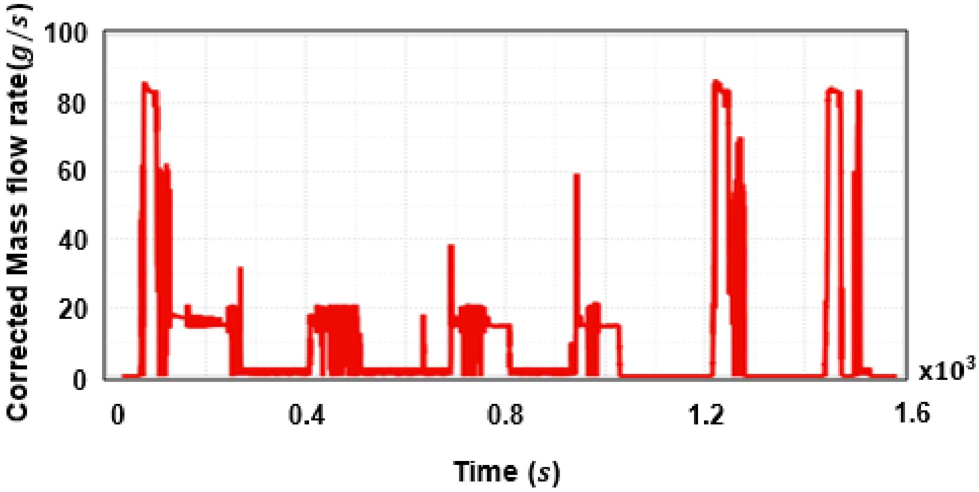

Fig. 3.10 Simulation result of air compressor corrected compressor speed

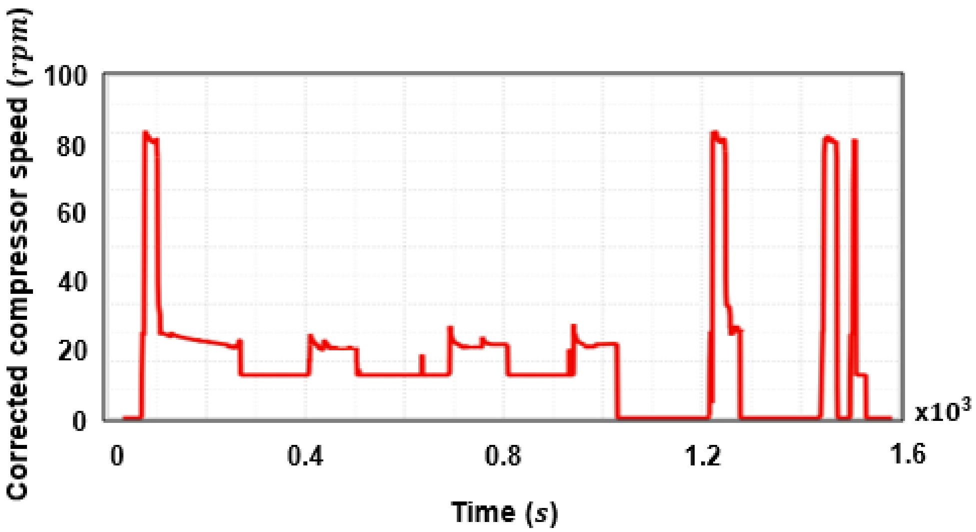

Additionally, by conducting a comparison with transient actual vehicle test data, the corrected mass flow rate and corrected compressor speed were calculated, as illustrated in Figs. 3.9 and 3.10.

Fig. 3.11 Simulation result of air compressor mass flow rate verification

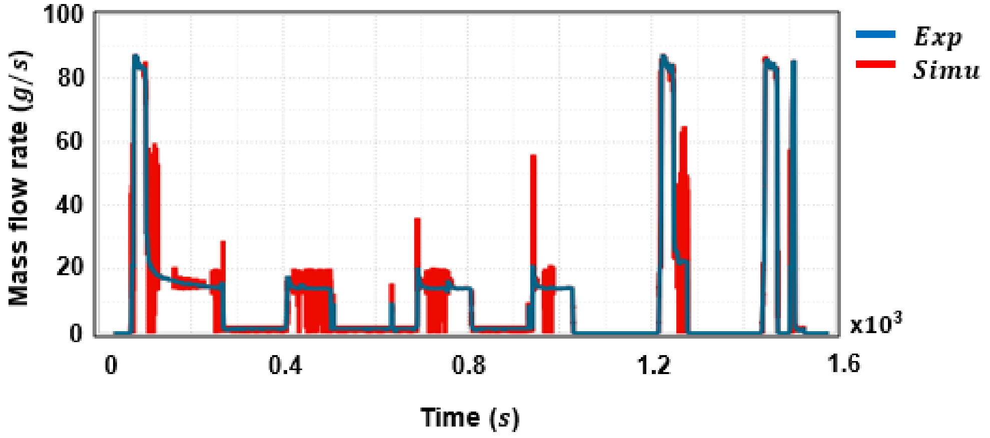

Fig. 3.12 Simulation result of air compressor pressure ratio verification

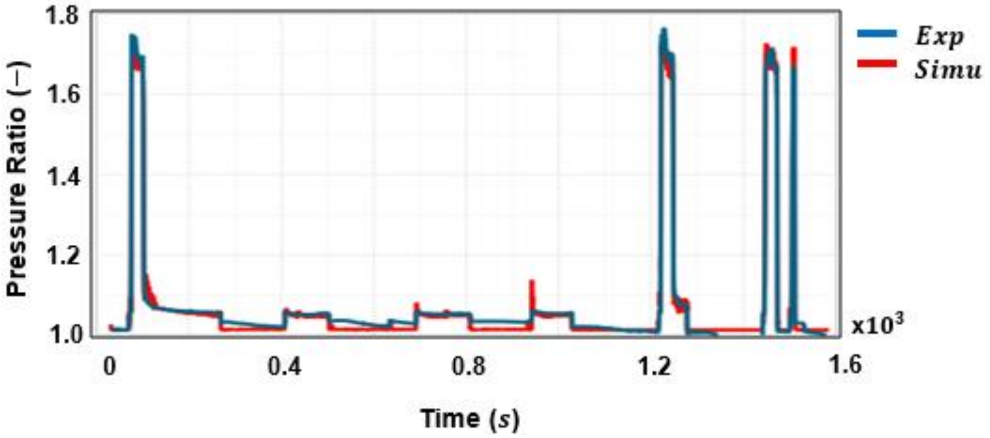

By determining the operating point using the map data, it was confirmed that the simulation values for the air mass flow rate closely followed the actual vehicle test results with an error of 1.2%, as shown in Fig. 3.11. Additionally, the pressure ratio was also simulated with an error of 1% in Fig. 3.12.

Fig. 3.13 Simulation result of air compressor outlet temperature verification

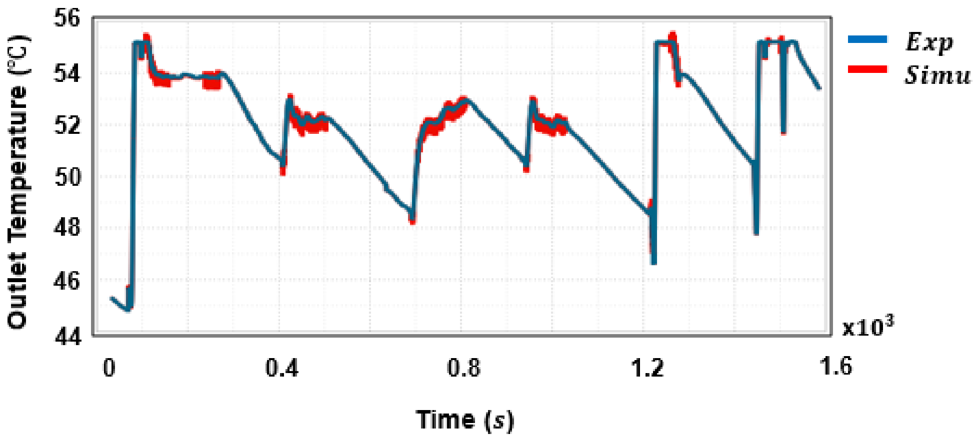

Fig. 3.14 Simulation result of air compressor isentropic efficiency

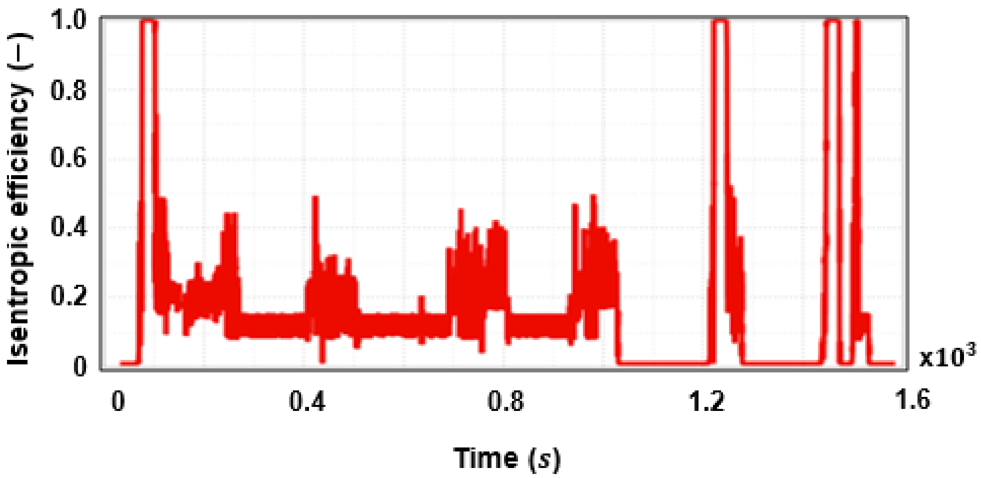

To accurately calculate the air compressor outlet temperature, the isentropic efficiency value was employed, carefully considering the operating point determined through the corrected value. The simulation results for the air compressor outlet temperature exhibited an impressive level of agreement with the actual vehicle test data, showcasing a remarkable error rate of merely 1%, as clearly depicted in Fig. 3.13. Furthermore, the isentropic efficiency value were determined, as shown in Fig. 3.14, which further validated the model's reliability and precision.

In essence, the meticulous model verification process for the air compressor served as a compelling testament to the effectiveness and accuracy of our simulation approach. The close alignment between the simulation results and the actual vehicle test data demonstrated the model's ability to capture the intricate dynamics of the air compressor under various operational conditions. This successful validation process instills confidence in the model's predictive capabilities, making it a valuable tool for assessing and optimizing the performance of the air compressor and, consequently, the overall fuel cell system in practical applications.

3.4 Verification of TMS model

The PEM fuel cell stack's TMS modeling consists of a coolant pump, and radiator with fan. The coolant pump was modeled by adjusting its rotational speed to provide an appropriate coolant mass flow rate. The radiator and fan were modeled by controlling the fan speed based on the heat generated by the PEM fuel cell stack and coolant mass flow rate to regulate the stack's temperature effectively.

To validate the TMS simulation model, it was compared and verified against the results of FCEB dynamometer vehicle tests. By comparing the simulation results with the real-world vehicle test data, the accuracy and reliability of the TMS model were confirmed.

In summary, the TMS model for the PEM fuel cell stack includes the coolant pump, radiator with fan. The pump's rotational speed is adjusted to achieve the desired coolant flow rate, while the radiator and fan are controlled based on the heat generated by the PEM fuel cell stack to maintain the stack at an appropriate temperature. The model's accuracy was validated through comparison with FCEB dynamometer vehicle test results, ensuring its effectiveness in predicting and managing the PEM fuel cell stack's thermal behavior.

Fig. 3.15 Verification model vehicle speed

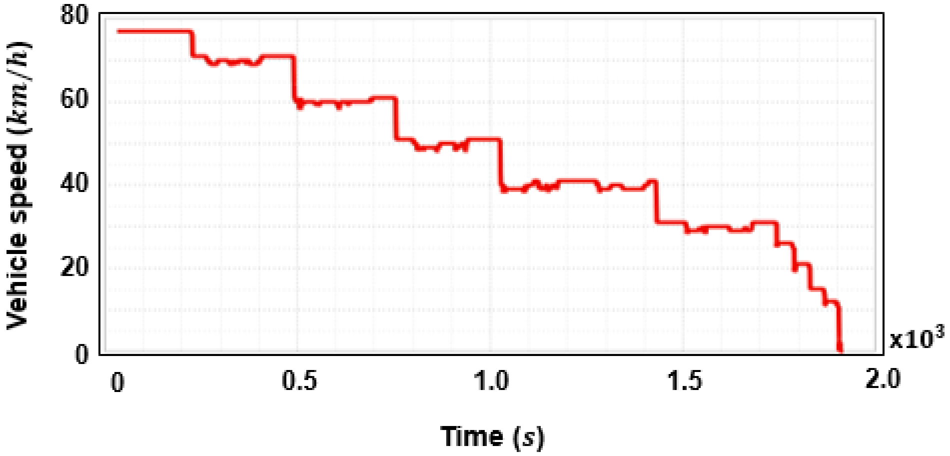

Fig. 3.16 Verification model stack power and heating rate

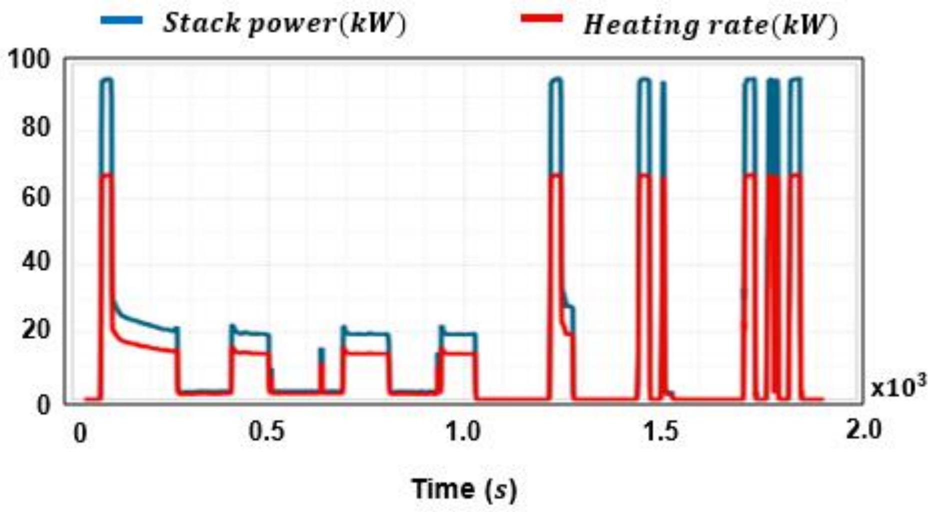

Figs. 3.15 and 3.16 display the vehicle speed, stack power, and heating value of the fuel cell stack used in the test mode. During the test, the vehicle's maximum speed was gradually reduced, and variations were made to the motor and fuel cell stack power.

Fig. 3.17 Simulation result of coolant mass flow rate verification

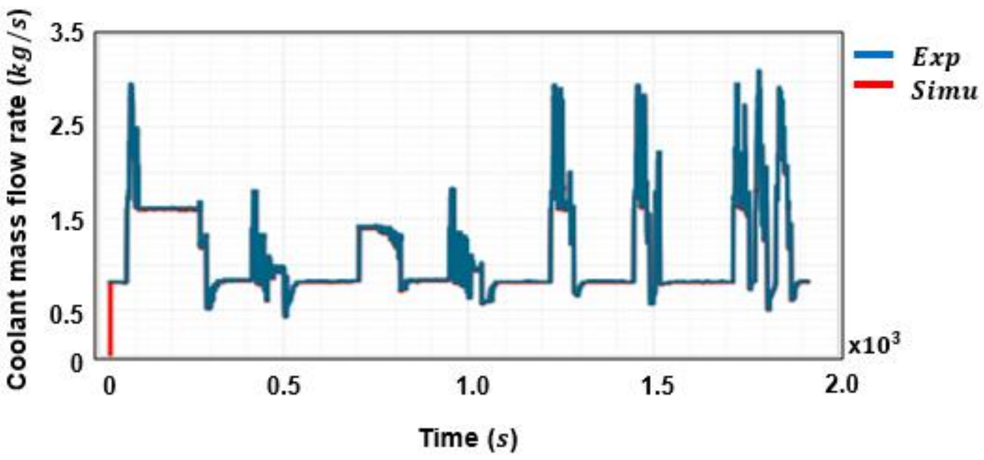

As depicted in Fig. 3.17, the coolant mass flow rate was modeled by adjusting the coolant pump speed to match the test value's flow rate.

Fig. 3.18 Simulation result of PEM fuel cell stack coolant inlet temperature verification

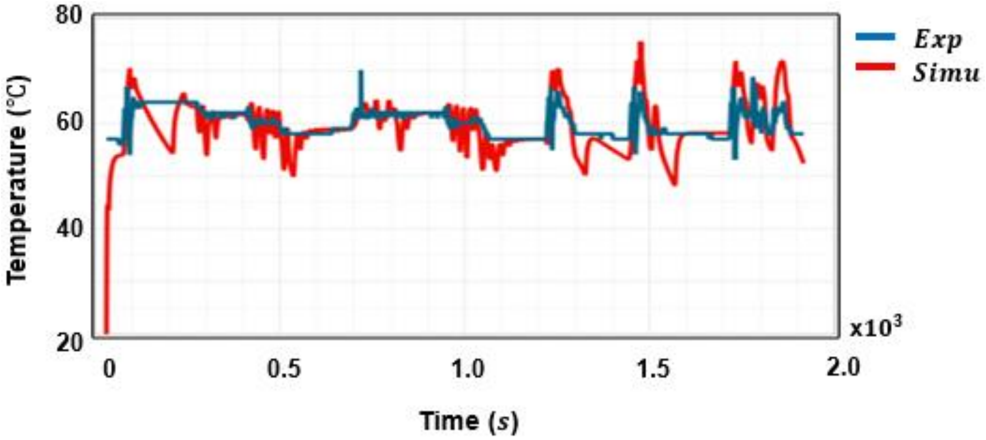

Fig. 3.19 Simulation result of PEM fuel cell stack coolant outlet temperature verification

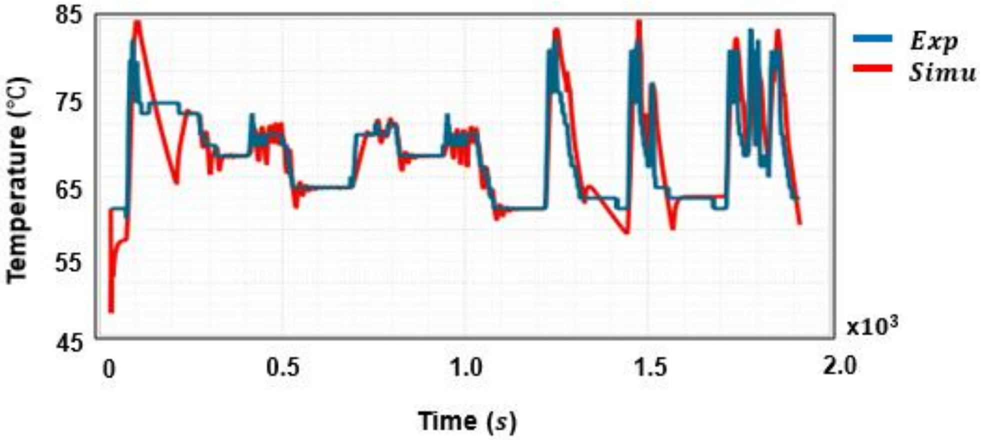

Figs. 3.18 and 3.19 display the inlet and outlet temperatures of the coolant passing through the stack, with both the measured and modeled values presented. The modeling results for coolant temperature exhibited an average error of 2.6% and 2.7% in comparison to the test data, respectively. It is worth noting that the majority of the errors occurred within the initial 300 seconds after the test commenced. However, once the system reached a stabilized state, the error remained within 2%, indicating a good agreement between the modeled and measured values during steady-state operation.

Fig. 3.20 Simulation result of radiator coolant inlet temperature verification

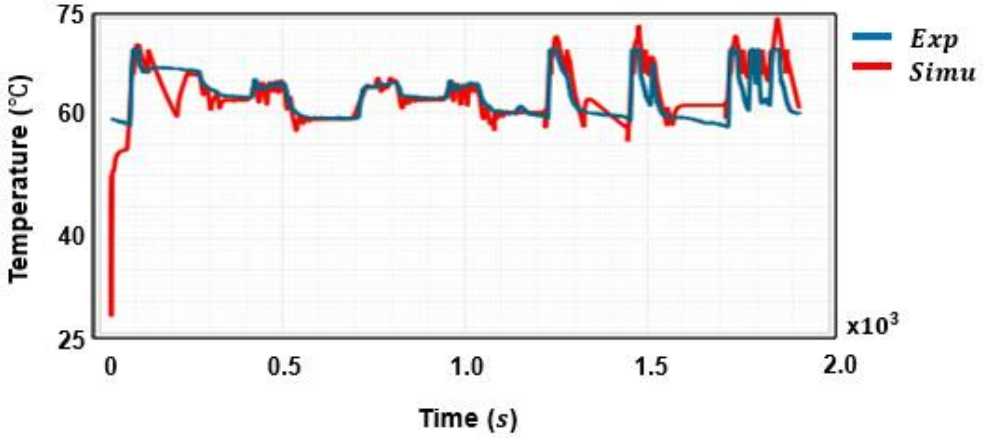

Fig. 3.21 Simulation result of radiator coolant outlet temperature verification

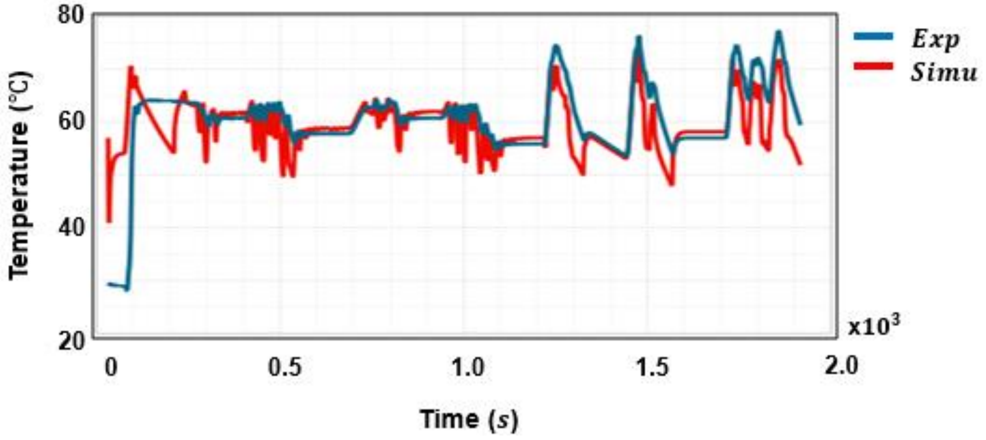

As the coolant flows through the fuel cell stack, it undergoes heat exchange and releases heat to the surroundings while passing through the radiator and the oil pump. The heat dissipation in the radiator is influenced by the relationship between the mass flow rate of the coolant and the air speed passing through the radiator. The temperature of the coolant as it passes through the radiator is depicted in Figs. 3.20 and 3.21. The modeling results for coolant temperature showed an average error of 2.1% and 3.4% when compared to the test data, respectively. Despite some deviations, the modeling results still exhibit a relatively good agreement with the experimental data, providing valuable insights into the thermal behavior of the coolant during its flow through the radiator.

Fig. 3.22 Simulation result of PEM fuel cell stack temperature

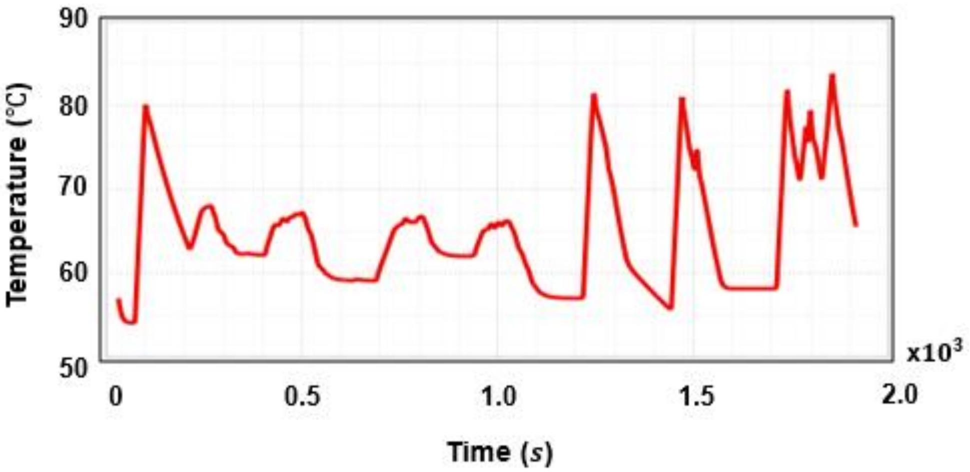

Furthermore, the simulation result for the PEM fuel cell stack temperature is observed in Fig. 3.22.

3.5 FCEB system energy flow

In this fuel cell system, various devices consume power, including the BOP systems. These BOP systems draw power from high-voltage battery packs, but they also utilize a portion of the power generated by the PEM fuel cell stack to support components with high power consumption. As a result, there is a loss of power from the PEM fuel cell stack, which is critical to consider when testing and verifying the PEM fuel cell stack's specifications. Therefore, understanding the power consumption of each BOP system becomes essential, and this analysis is conducted through dynamometer vehicle tests and modeling.

By conducting dynamometer vehicle tests and modeling simulations, the overall energy flow during FCEB driving is thoroughly analyzed. The total power in the FCEB system is the combined sum of the PEM fuel cell stack power and the battery power. Additionally, this sum of powers equals the total power consumed by the bus's drive motor and other BOP systems. The motor's efficiency is assumed to be 90%. The demanded power for the FCEB is determined using a specific equation.

Following the dynamometer vehicle tests, the power consumed by each BOP system is measured using current and voltage sensors. Based on the test results, a relational expression is established, relating the power consumed in each BOP system to the fuel cell stack power and temperature.

Leveraging the results of the PEM fuel cell stack power analysis, two relatively steady-state sections were identified. Consequently, the energy flow for different power outputs was calculated, taking into account both the power generated by the

PEM fuel cell stack and the power consumed by the BOP systems under various driving conditions. This comprehensive analysis, combining dynamometer vehicle tests and modeling simulations, enables valuable insights into the power distribution and usage within the FCEB system. Moreover, it facilitates a deeper understanding of the PEM fuel cell stack's performance and efficiency in real-world operating conditions.

Table. 3.4 FCEB system energy flow (FC stack 19.4 kW)

	Power (kW)		Percent (%)
Stack_power	38.86	70.36	100
Battery_power	31.5		
Motor_power	62.9		89.4
Others_power	3.35		4.76
Batt_comp_power	1.89		2.7
FC_comp_power	1.11		1.58
FC_pump_power	0.72		1.02
FC_oil_power	0.39		0.55
Batt_fan_power	0.01		0.014
Batt_pump_power	0.006		0.01

Fig. 3.23 Simulation result of FCEB energy flow (FC stack power 19.4 kW)

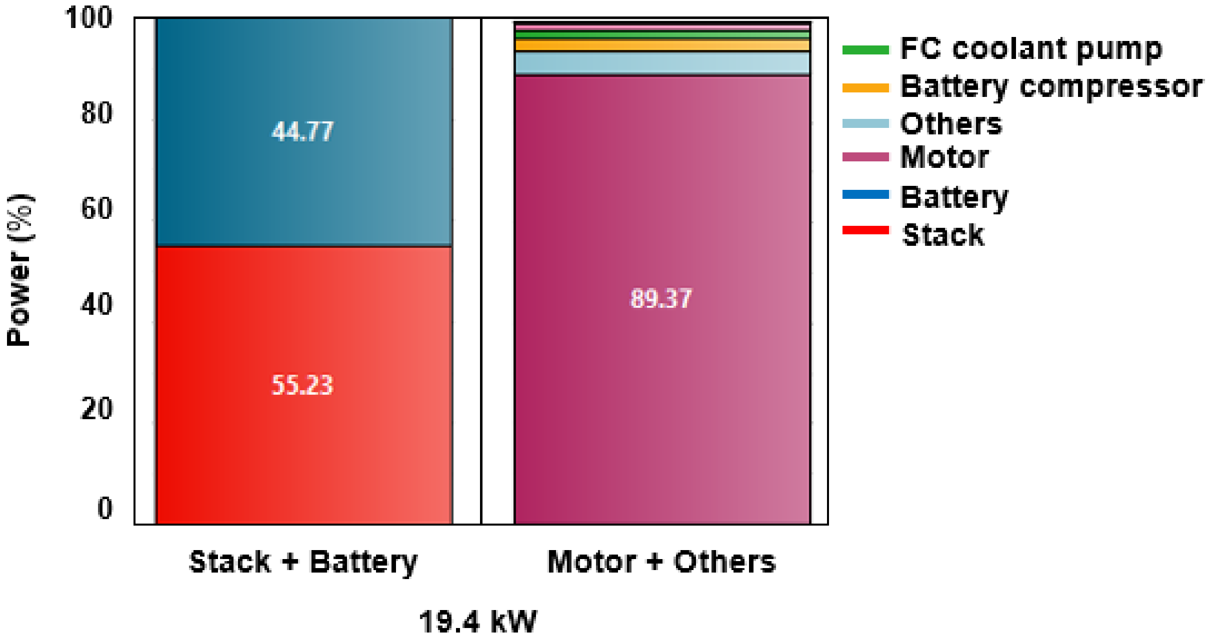

In the section where the fuel cell stack power is 19.4 kW, it corresponds to a relatively low load operating condition. At this specific point, 55% of the total power is supplied by the fuel cell stack, while the remaining 45% is drawn from the high-voltage battery. This combined power is then efficiently distributed to both the electric motor and the BOP system.

Within this section, the BOP system's primary power consumers are the air compressor in the fuel cell and the battery refrigerant compressor in the battery pack. The fuel cell, operating at lower power levels, requires relatively minimal power for cooling from the coolant pump or the oil pump radiator.

However, in the case of the battery system, continuous power is required due to ongoing battery discharge, resulting in a rise in the battery system's temperature due to heat generated during battery operation. Consequently, a substantial amount of power is crucially needed from the battery refrigerant compressor to effectively manage and dissipate the heat produced by the battery.

The results of the energy flow simulation are detailed in Table 3.4, while Fig. 3.23 visually presents the distribution of power and energy flow during this specific low load section of the fuel cell system. These simulation results provide valuable insights into the power distribution, system behavior, and thermal management aspects during this operating condition, contributing to a deeper understanding of the overall system performance.

Table. 3.5 FCEB system energy flow (FC stack 90.0 kW)

	Power (kW)		Percent (%)
Stack_power	180	202.64	100
Battery_power	22.64		
Motor_power	156.76		73.44
FC_oil_power	24.25		11.36
FC_comp_power	20.86		9.77
Others_power	7.23		3.39
FC_pump_power	2.42		1.13
Batt_comp_power	1.89		0.89
Batt_pump_power	0.013		0.01
Batt_fan_power	0.01		0.005

Fig. 3.24 Simulation result of FCEB energy flow (FC stack power 90.0 kW)

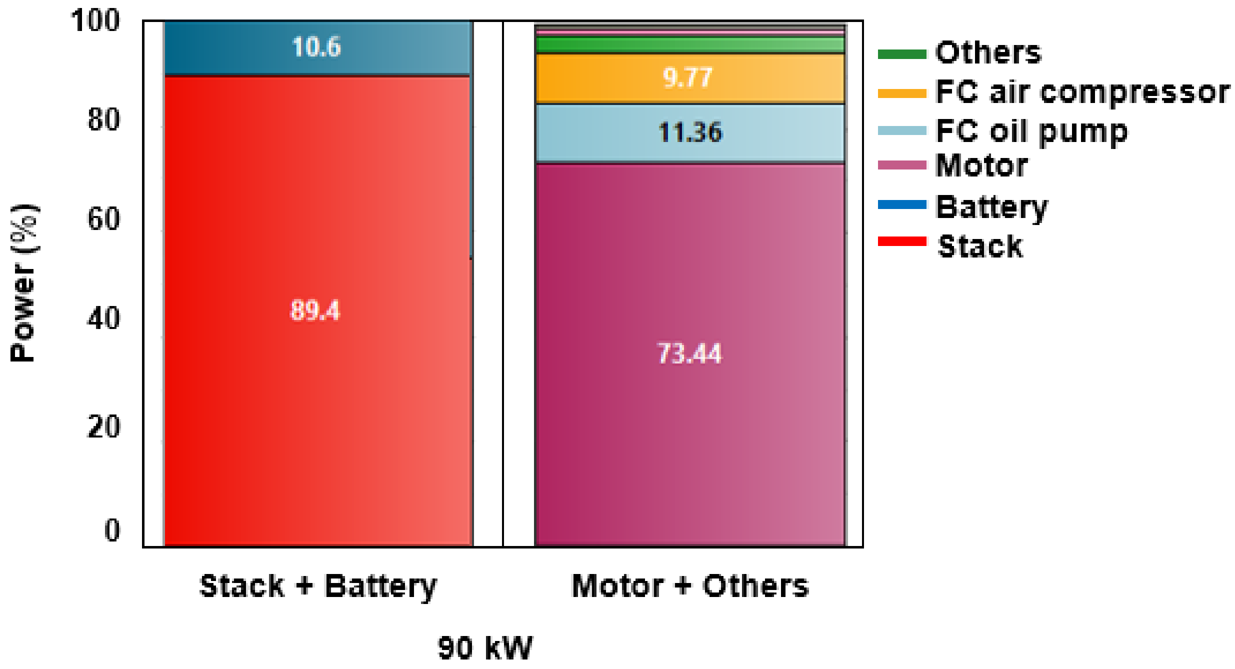

At a PEM fuel cell stack power of 90 kW and a battery State of Charge (SOC) of approximately 25%, it became apparent that the stack was generating more power than needed to charge the battery. In this scenario, the stack oil pump radiator and the air compressor emerged as the BOP system's highest power consumers. As the stack power increased, it also led to a proportional rise in heat generation, resulting in higher power consumption by the cooling system. Particularly, the power consumption of the oil pump saw a significant increase.

While the power consumption of the battery TMS remained relatively stable compared to the partial load condition, the intensified power usage in the stack cooling system caused the percentage of total power consumption attributed to the battery to decrease.

The outcomes of the energy flow simulation are summarized in Table 3.5, while Fig. 3.24 visually illustrates the distribution of power and energy flow during this specific scenario. These simulation results provide valuable insights into the power distribution, thermal dynamics, and overall system behavior during a high power output condition, with the fuel cell stack and battery operating at different power levels.

Chapter 4. Conclusion

In this study, the Simcenter AMESIM-based 0-D modeling program was employed to simulate the PEM fuel cell system, encompassing the PEM fuel cell unit cell and stack, along with the BOP system containing the air compressor, humidifier, and TMS. The PEM fuel cell unit cell model was developed and verified by comparing polarization curves based on temperature, pressure, and relative humidity from experiments and simulations, showing excellent agreement between the simulation results and experimental data.

For the PEM fuel cell stack, multiple unit cells were stacked to generate the required power. The stack model's accuracy was validated by comparing simulation results with transient data from FCEB dynamometer vehicle tests, revealing a close match between the polarization curve obtained from the simulation model and the test results.

Furthermore, special attention was given to modeling the air compressor, a critical component responsible for supplying air at the appropriate flow rate and pressure for the fuel cell stack's electrochemical reactions. The air compressor was modeled using pressure ratio and isentropic efficiency data maps, and its performance was verified by comparing temperature and pressure data from the simulated model with real-world test data, resulting in favorable agreement between simulation and test results.

The TMS, comprising a coolant pump and an oil pump radiator, was also modeled in the study. The coolant pump's flow rate was controlled by adjusting its speed, while the oil pump radiator's fan velocity was regulated to achieve effective heat dissipation based on the coolant flow rate and heating value. The TMS model was validated by comparing flow rate and temperature data at the front and rear ends with data obtained from FCEB dynamometer vehicle tests, showing excellent correlation between simulation and test data.

To evaluate the overall fuel cell system, power and power consumption values of each component were calculated. The total power in the fuel cell vehicle system is the combined sum of the fuel cell stack power and the battery power. These two powers together equal the sum of the powers consumed by the vehicle's driving motor and other BOP systems. By analyzing the stack power results, two relatively stable sections were identified, and the energy flow at these power levels was analyzed, with simulation results closely matching dynamometer vehicle test data.

In conclusion, this study successfully developed and validated models for various components of the PEM fuel cell system, demonstrating their accuracy in predicting performance and energy flow under real-world conditions.

Bibliography

[1] Alaswad A, Baroutaji A, Carton J, Makky Ahmed Al, Olabi A.G. Developments in fuel cell technologies in the transport sector. (2016). Journal of Hydrogen Energy, 41, 16499-16508.

[2] Guangjin Wang, Yi Yu, Hai Liu, Chunli Gong, Sheng Wen, Xiaohua Wang, Zhengkai Tu. Progess on design and development of polymer electrolyte membrane fuel cell systems for vehicle applications: A review. (2018). Fuel Processing Technology, 179, 203-228.

[3] Yuanyang Zhao, Yunxia Liu, Guangbin Liu, Liansheng Li, Zhicheng Gao. Air and hydrpgen supply systems and equipment for PEM fuel cells: A review. (2022). Journal of Green Energy, 19:4, 331-348.

[4] Soohwan Kim, Hoyoung Jeong, Hoseong Lee. Cold-start performance investigation of fuel cell electric vehicles with heat pomp-assisted thermal management systems. (2021). Journal of Energy, 232, 121001.

[5] Huei Peng, Dongmei Chen. A thermodynamic model of membrane humidifiers for PEM fuel cell humidification control. (2005). Journal of Dynamic Systems 127, 426-427.

[6] SangKyun Park, SongYul Choe. Dynamic modeling and analysis of a shell-and-tube. (2008). Journal of Hydrogen Energy 33, 9, 2273–2282.

[7] Alexander Proracki. Predictive Modeling of a PEMFC Cathode Humidifier. (2010). University of Waterloo, 3-100.

[8] Mulyazmi, W.R.W. Daud. Water balance for the design of a PEM fuel cell system. (2012). Journal of Hydrogen Energy 38, 22, 9409–9420.

[9] Cong Yin, Hao Tang. Review of System Integration and Control of Proton Exchange Membrane Fuel Cells. (2020). Journal of Springer 3, 466–505.

[10] JoonYoung Hwang. Mass and Heat Transfer Analysis of Membrane Humidifier with a Simple Lumped Mass Model. (2009). Journal of Mechanical Science and Technology 33, 8, 596–603.

[11] Fengxiang Chen, Yaowang Pei. Analysis of Influencing Factors on Dynamic Performance of PEMFC Air Supply System. (2020). Journal of IEEE, 64–68.

[12] Yuemeng Zhang. Modeling and analysis of air supply system of polymer electrolyte membrane fuel cell system. (2017). Journal of Energy Procedia 142, 1053–1058.

[13] JeongHo Lee. The Effect of Thermal Management on the Performance of a Polymer Electrolyte Membrane Fuel Cell System. (2011). Journal of Mechanical Science and Technology 35, 6, 593–601.

[14] SangGyu Kang. Dynamic Simulation of A Stationary PEM Fuel Cell System. (2006). Journal of Mechanical Science and Technology, 1810–1815.

[15] Jay Tawee Pukrushpan. Modeling and control of fuel cell systems and fuel processors. (2003). University of Michigan, 5–133.

[16] HanSang Kim. A Study on the Analysis of the Performance and Efficiency of a Low-pressure Operating PEMFC System for Vehicle Applications Using MATLAB/Simulink. (2013). Journal of Hydrogen and New Energy 24, 5, 393– 400.

[17] HanSang Kim. A Study on the Simplified Performance Modeling of Automotive PEMFC System by Using MATLAB/Simulink Environment. (2011). The Korean Society Of Automotive Engineers, 2948–2953.

[18] HanSang Kim. Modeling of PEM Fuel Cell System–Sensitivity Analysis of System Efficiency with Different Main Operating Parameters of Automotive Fuel Cell System. (2005). Journal of Korean Hydrogen and New Energy Society 30, 5, 401-410.

[19] Jørgen Kristoffer Tuset. Modelling and Validation of a Fuel Cell Electric Bus. (2021). University of Oslo, 1-60.

[20] Trung V. Nguyen, Ralph E. White. A Water and Heat Management Model for Proton-Exchange-Membrane Fuel Cells. (1993). Journal of Electrochemical Society 140, 8, 2179-2181.

[21] SangKyun Park, Song-Yul Choe, Seo-ho Choi. Dynamic modeling and analysis of a shell-and-tube type gas-to-gas membrane humidifier for PEM fuel cell applications. (2008). Journal of Hydrogen energy 33, 2275-2276.

[22] Shoaib Khanmohammadi, Mohammad Rahmani, Farayi Musharavati, Saber Khanmohammadi, Quang-Vu Bach. Thermal modeling and triple objective

optimization of a new compressed air energy storage system integrated with Rankine cycle, PEM fuel cell, and thermoelectric unit. (2021). Journal of Sustainable Energy Technologies and Assessments 43, 5-7.

[23] SangGyu Kang. Dynamic simulation of a fuel cell hybrid vehicle during the federal test procedure-75 driving cycle. (2016). Journal of Applied Energy 161, 181–196.

[24] Himadri Chattopadhyay. Analysis of flow structure inside a spool type pressure regulating valve. (2012). Journal of Energy Conversion and Management 53, 196–204.

[25] Joel Björkman. Development of pump geometry for engine cooling system. (2015). KTH School of Industrial Engineering and Management, 2–79.

[26] Samson Solomon. Prediction of Thermal Performance of Radiator Using 1-D Method. (2013). SAE Technical Paper, 2013-01-2810.

국문 초록

수소전기버스 고분자전해질 연료전지 시스템 모델링

서울대학교 기계공학부

기계공학과

김 영 섭

연료전지와 배터리를 하이브리드 방식으로 탑재한 수소연료전기버스는 친환경성, 저소음과 같은 특성을 보이며, 수소충전 및 유지관리 인프라 간소화에도 강점이 있어 최근 각광받고 있다. 또한 수소의 높은 에너지 밀도 값은 차량의 에너지 저장 용량 및 차량 주행 거리 향상에 도움을 주어 트럭, 버스 및 기타 운송수단 등에 적용성이 높다.

수소전기버스의 고분자전해질 연료전지는 연료인 수소가 가진 화학적 에너지를 전기적 에너지로 변화시켜 사용하는 에너지 변환장치로써 전기화학 반응의 결과 부산물로 물과 열이 생성된다. 연료전지 시스템은 연료전지 스택과 주변운전장치로 구성된다. 주변운전장치는 반응기체인 산소와 수소를 공급하기 위한 공기 공급 시스템, 수소 공급 시스템과 연료전지 열방출을 통해 60~80℃의 운전온도를 유지하기 위한 열관리 시스템으로 구성된다.

이러한 연료전지 시스템을 구성하는 각각의 시스템은 서로 열·전기적현상에 의해 상호작용하며, 고분자전해질 연료전지 시스템의 체계적인 해석 및 시스템을 구성하는 다양한 시스템의 효율적인 제어를 하기 위해서는 시스템을 구성하는 각 요소들에 대한 물리적인 분석과 이를 모두 반영한 모델링이 수행되어야 한다. 본 연구에서는 각 구성 요소들에 대한 물리적인 현상 및 지배방정식을 이해하고 AMESIM®을 이용하여 연료전지 시스템 모델로 통합하고자 한다. 구축한 모델은 차량 실험 데이터와의 비교를 통해 검증되었다.

주요어: 수소전기버스, 고분자전해질 연료전지, 연료전지 운전장치, 시뮬레이션

학번: 2021-24465